The Seasonal Variation of the Tropical Circulation as Simulated by a Global Model of the Atmosphere

SYUKURO MANABE, DOUGLAS G. HAHN AND J. LEITH HOLLOWAY, JR.

Geophysical Fluid Dynamics Laboratory, NOAA, Princeton University, Princeton, N.J. 08540

(Manuscript received 16 July 1973)

ABSTRACT

A mathematical model of the atmosphere with a seasonal variation of insolation and sea surface temperatures is integrated numerically with respect to time over three model years. The model has a global computational domain and a realistic distribution of mountains. It contains a highly idealized parameterization of convection, i.e., dry and moist convective adjustment.

It is found that the model accurately simulates the seasonal variation of the location of the tropical rainbelt as well as that of the flow field associated with it. Over the continental regions of the model, the tropical rainbelt tends to form very close to the equator, whereas, in certain oceanic regions, it has a tendency to form away from the equator. Based upon a comparison of these results with those of another numerical experiment, it is concluded that this tendency is not due to an inherent characteristic of the rainbelt of the model to avoid the equator in oceanic regions, but rather it is due to the equatorial belt of low sea surface temperatures which is not favorable for the formation of a rainbelt. Over the sea, the surface temperature distribution seems to be the primary factor in determining the location of the rainbelt and accompanying tropical disturbances.

The primary source of kinetic energy of the disturbances in the model tropics is the conversion of eddy available potential energy which is generated by the effects of moist convection. A secondary source is the energy supplied from middle latitudes through pressure interaction. This effect has a significant magnitude in the subtropics of the model. The belt of maximum eddy conversion moves from one summer hemisphere to the other with respect to season in a manner similar to the tropical rainbelt. On the other hand, the contribution of pressure interaction to the production of eddy kinetic energy is significant in the winter hemisphere and thus supplements the contribution of eddy conversion. In general, the rate of eddy conversion due to transient eddies is particularly large in areas of relatively warm sea surface temperatures, where the tropical rainbelt and its accompanying disturbances predominate.

1. Introduction

For the past two decades, many attempts have been made to simulate the general circulation of the tropics with mathematical models of the atmosphere. Using a quasi-geostrophic, two-level general circulation model, Phillips (1956) reproduced qualitatively a direct Hadley cell in the tropics and an indirect Ferrel cell in middle latitudes. Smagorinsky (1963) constructed a "primitive equation" model which paved the way for the successful simulation of the tropical general circulation. Mintz (1965) constructed a model of the atmosphere with a global computational domain and realistic topography. Although he obtained a highly realistic distribution of sea level pressure in middle latitudes, the horizontal flow field in his model tropics is not very realistic. Particularly, the intertropical convergence zone is located too far away from the equator and the intensity of the convergence is very weak.

The models mentioned so far do not explicitly incorporate the processes associated with the hydrologic cycle. Parameterizing the effects of moist convection by the so-called "moist convective adjustment," Manabe *et al.* (1965) constructed a hemispheric model with moist processes which simulated the basic features of the latitudinal distribution of precipitation, such as the tropical rainbelt, the subtropical dry zones, and the rainy belt in middle latitudes. They demonstrated that the rainbelt in the model tropics resulted from many centers of intense precipitation associated with synoptic-scale disturbances, such as tropical cyclones and easterly waves, in agreement with the features of the actual intertropical convergence zone (Manabe and Smagorinsky, 1967). According to their analysis, these synoptic-scale disturbances have a warm core in the upper troposphere and are maintained by the conversion of eddy available potential energy generated by the heat of condensation. Bates (1970) constructed a quasi-geostrophic general circulation model of the tropics in which the east-west variation of variables is represented by a truncated Fourier series. In his model, disturbances with a wavelength of about 2000 km occupy the intertropical convergence zone (ITCZ). These disturbances have a warm core structure and a maximum amplitude

in the lower troposphere. At the mature stage of development of the ITCZ, the kinetic energy of the disturbances is provided mainly by the direct conversion of eddy available potential energy generated by condensation, agreeing with the results of Manabe and Smagorinsky (1967).

In Bates' model, the ITCZ is located away from the equator. Earlier, Charney (1966) concluded that the ITCZ should not form over the equator based upon his theoretical study on the growth rate of the ITCZ. The conclusions of these studies differ from those of Manabe (1969a). Using a three-dimensional model with a limited longitudinal span and a coarse computational grid mesh, Manabe showed that the ITCZ tends to form along the equator, unless it is surpressed by an underlying belt of cold sea water [see Manabe (1969b) and Bryan (1969)]. Similar numerical results are obtained by Pike (1970) from a two-dimensional model of the tropics with very good computational resolution. The disagreements among the results described above indicate a need for further study of this subject.

The models of Manabe, Bates and Pike have limited computational domains. An attempt to construct a model with a global computational domain and realistic topography has been made by Manabe *et al.* (1970). Using the insolation at the top of the atmosphere and the observed sea surface temperatures in January as boundary conditions, their model simulates some of the essential features of the January mean flow field and rainfall distribution in the tropics. Kasahara and Washington (1971) also performed a similar numerical experiment and were able to simulate successfully some of the zonal mean features of the water and heat budgets in the model tropics.

According to Manabe *et al.* (1970), the kinetic energy of not only the tropical cyclones but also that of very long waves in the model tropics is essentially maintained against dissipation by the release of available potential energy. This is in agreement with the results from the observational studies by Nitta (1970) as well as from the earlier study by Manabe and Smagorinsky (1967). [Also, see the theoretical studies of Yamasaki (1969), Hayashi (1970) and Krishnamurti (1969)]. However, the energy supplied from middle latitudes through pressure interaction also contributes significantly to the production of eddy kinetic energy in their model's subtropics, agreeing with Mak's (1969) theoretical study.

Encouraged by the success in simulating the climate of January, we have attempted to numerically simulate the seasonal variation of the general circulation of the atmosphere. Despite the extreme simplifications adopted for parameterizing the moist convective processes, the basic features of the seasonal variation of the general circulation in the tropics are successfully simulated by the model. Therefore, it is decided to present a detailed analysis of the model tropics. Special emphasis of this study is placed not only upon the analysis of the location of the ITCZ but also upon the examination of the seasonal variation of the energetics of tropical disturbances. For a detailed spectral analysis of the transient disturbances appearing in this model, see Hayashi (1973).

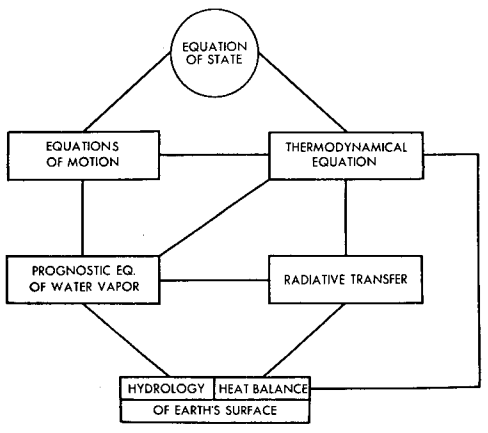

FIG. 2.1. Schematic diagram indicating the model structure.

2. Brief description of the model

The global model used for this study is very similar to the model described by Holloway and Manabe (1971) except that it undergoes a seasonal variation. Therefore, only a brief sketch of the model is given here. To supplement the following description of the model, a box diagram, which illustrates the major components of the model and the interaction among these components, is presented in Fig. 2.1.

The model incorporates the primitive equations of motion in a spherical coordinate system. The numerical problems associated with the treatment of mountains are minimized by using the sigma coordinate system in which pressure, normalized by surface pressure, is the vertical coordinate (Phillips, 1957). In order to simulate the effects of subgrid-scale mixing, a nonlinear viscosity is added to the model as suggested by Smagorinsky (1963). The finite-difference form of the dynamical equations is similar to that proposed by Kurihara and Holloway (1967). A global grid system is chosen such that the horizontal grid size of approximately 250 km is as uniform as possible. Fig. 2.2 shows a part of the horizontal grid system. In the vertical direction, 11 finite-difference levels are chosen so that the model can simulate the structure of the stratosphere as well as that of the planetary boundary layer. The normalized pressure and approximate height of these eleven levels are given in Table 1.

The scheme for computing radiative heating and cooling is identical with that described by Manabe and Strickler (1964) and Manabe and Wetherald (1967). It consists of two parts, i.e., solar radiation

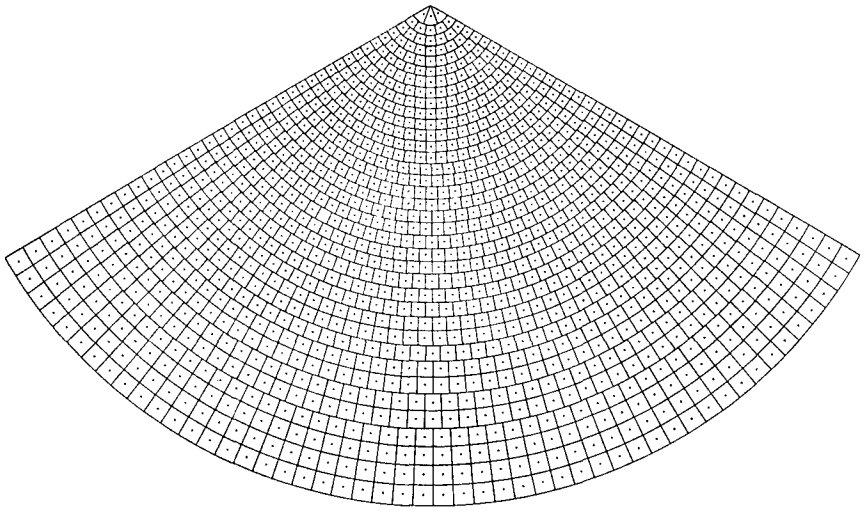

FIG. 2.2. A polar stereographic projection of one-sixth of the global horizontal grid system bounded by 1.2S and two meridians 120° apart. Grid points are represented by dots at the centers of the grid boxes.

and longwave radiation. The solar radiation at the top of the atmosphere is a function of latitude and season; however, its diurnal variation is eliminated for the sake of simplicity. The seasonal variation of insolation is controlled by changes in both the declination of the sun and its distance, which are functions of the date. An annual mean observed distribution of clouds, which varies with latitude and height, but not with longitude, is used in the computation of radiative transfer. Three atmospheric gases are also taken into consideration for the computation of radiative transfer: water vapor, ozone and carbon dioxide. The distribution of water vapor is computed by a prognostic system described later. An observed distribution of ozone, which varies with season, latitude and height, is used for this computation. The mixing ratio of carbon dioxide is assumed to have a constant value of 0.456×10^{-3} everywhere.

The surface temperature over land is determined by the boundary condition that no heat be stored in the ground, i.e., net fluxes of solar and terrestrial radiation and the turbulent fluxes of sensible and latent heat all locally add to zero. Over the oceanic part of the model, the seasonal variation of surface temperature is prescribed. It is determined by interpolating in time between four observed distributions of monthly mean sea surface temperatures, i.e., means for February, May, August and November. Data from the *World Atlas of Sea Surface Temperatures*, which has been recently revised by the Hydrographic Office (1964), are used for this purpose.

TABLE 1. Values of vertical coordinate (σ) and the corresponding standard heights (approximate values) for each of the 11 vertical finite difference levels.

Level	σ	Height (standard) (km)
1	0.010	30.93
2	0.038	22.21
3	0.065	18.79
4	0.110	15.45
5	0.190	11.98
6	0.315	8.67
7	0.500	5.44
8	0.685	3.06
9	0.835	1.49
10	0.940	0.52
11	0.990	0.08

The prognostic system of water vapor consists of the contributions by the three-dimensional advection of water vapor, evaporation from the earth's surface, vertical mixing of water vapor in the planetary boundary layer, nonconvective condensation, and so-called "moist convective adjustment." In view of our lack of knowledge of the interaction between small-scale convection and the large-scale fields of momentum, temperature and moisture, we adopted an extremely idealized scheme of parameterizing the moist convection. This scheme, called moist convective adjustment, is executed wherever supersaturation and a super moist-adiabatic lapse rate exist. In the layer of moist convective adjustment, it is assumed that free convection is strong enough to make the equivalent potential temperature and the relative humidity constant with height.[1] In short, the moist convective process neutralizes the lapse rate, releases the heat of condensation, and transfers heat upward. It creates a warm core in the upper troposphere and a cold core in the lower

[1] It would have been possible to make the scheme of moist convective adjustment more realistic by introducing a critical relative humidity which is less than saturation. In this case, it is assumed that the partial equivalent potential temperature (corresponding to this new critical humidity) becomes constant in a moist convective process. Accordingly, the critical lapse rate falls somewhere between the dry and moist adiabatic lapse rates.

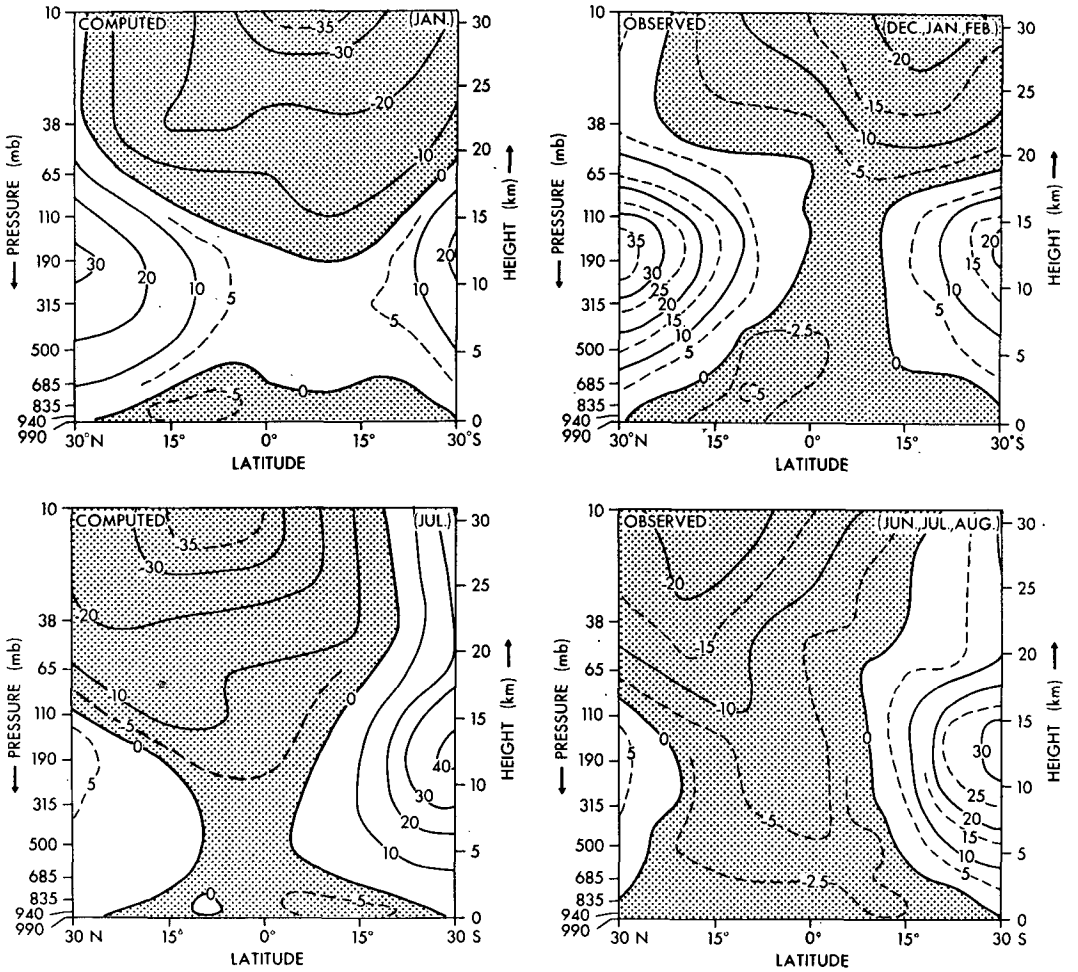

FIG. 3.1. Latitude-height distributions of mean zonal wind (m sec^{-1}) in low latitudes: left half, 1-month mean distributions in the model atmosphere in January and in July; right half, 3-month mean observed distributions in the December–February and June–August periods.

troposphere, thus producing an environment favorable for the conversion of eddy available potential energy as pointed out by Manabe and Smagorinsky (1967). By neutralizing the lapse rate, the moist convective adjustment prevents convective instability of the first kind, which would result from an unstable stratification and cause grid-scale convection in the model atmosphere. Despite the many idealizations involved in this scheme, it enables us to successfully simulate some of the basic features of the tropical general circulation (Manabe *et al.*, 1970). For a more specific description of moist convective adjustment, see Manabe *et al.* (1965).

The schemes for computing the hydrology of the ground surface are similar to those described by Manabe (1969a). The rates of the change of soil moisture and snow depth are determined by the budget of water, snow and heat at the ground surface.

The numerical time integration of the model is continued for a period of approximately 3.5 model years. The initial conditions for this integration are the mean state attained by the long-term integration of a global model which had January insolation and sea surface temperatures as imposed boundary conditions. The first 1.5 model years is time-integrated on a grid with low horizontal resolution (~500 km). A high resolution (~250 km) grid is used for time integrating the final 2 model years. The results from the time integration of the final 1.5 model years are analyzed for this study. The various annual mean quantities, shown here, represent an average for the last model year. For the purpose of computing the declination and distance of the sun, this 3.5-year period is considered to begin in February 1962.

Examination of the annual march of various quantities indicates that they do not repeat themselves exactly in the same manner from one year to another. It is not clear whether this interannual variation is due to the transient behavior of the model originating from the imbalance of initial conditions, or whether it is due

to the natural variability in the model. Further extension of the period of time integration is required to settle this question.

3. Zonal mean state of model atmosphere

a. Zonal wind

Latitude-height profiles of the mean zonal wind in the model atmosphere, for the periods of January and July, are shown in Fig. 3.1. For comparison, quarterly mean observed distributions of zonal wind averaged over a period of 7 years (Newell *et al.*, 1972) are added to the same figure. In the model stratosphere, easterlies prevail. This is in qualitative agreement with the features of the actual atmosphere except that the easterlies are much too strong. In the upper troposphere of the model tropics, weak westerlies and weak easterlies appear in January and July, respectively, whereas easterly winds appear in both months in the actual atmosphere. In both hemispheres the simulated intensity of the subtropical jet does not agree perfectly with that in the actual atmosphere; however, the general distribution of isotachs is quite realistic.

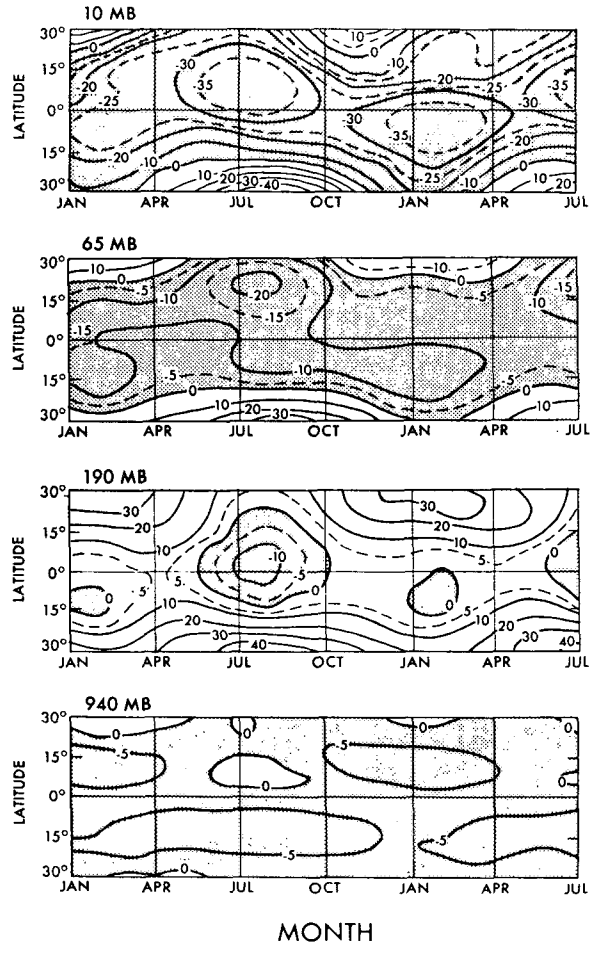

FIG. 3.2. Latitude-time distributions of zonal wind (m sec^{-1}) at the 10-, 65-, 190- and 940-mb levels in the model atmosphere.

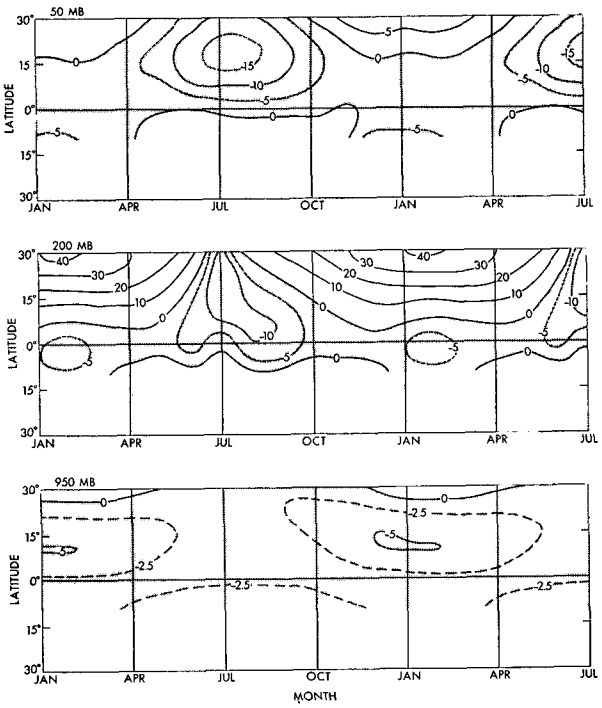

FIG. 3.3. Latitude-time distributions of zonal wind (m sec^{-1}) at the 50-, 200- and 950-mb levels in the actual atmosphere (Oort and Rasmusson, 1971). Note: last third of the figure is a repetition of the first.

The seasonal variation of the zonal wind at various isobaric levels of the model tropics is shown in Fig. 3.2. In the model stratosphere, the belt of maximum easterly wind moves from low latitudes of the Northern Hemisphere in August to low latitudes of the Southern Hemisphere in February. Similar features in the seasonal change are evident in the upper troposphere (190-mb level) although the belt of maximum easterly wind is located closer to the equator. In the lower troposphere of the model, the annual migration of the belt of maximum easterly wind moves in a manner opposite to that of the upper troposphere, i.e., maximum easterlies tend to appear in the Southern Hemisphere around July, and in the Northern Hemisphere around January. In October and April, maxima in the easterly wind coexist in both hemispheres separated by a minimum at the equator. In general, at latitudes very close to the equator, semiannual components are a very significant part of the seasonal variation of the zonal wind. The general features of the seasonal variation of zonal wind in the model tropics are in excellent qualitative agreement with those of the actual tropics, shown in Fig. 3.3. The observed distributions by Oort and Rasmusson (1971) are based upon data covering the 5-year period from May 1958 to April 1963.

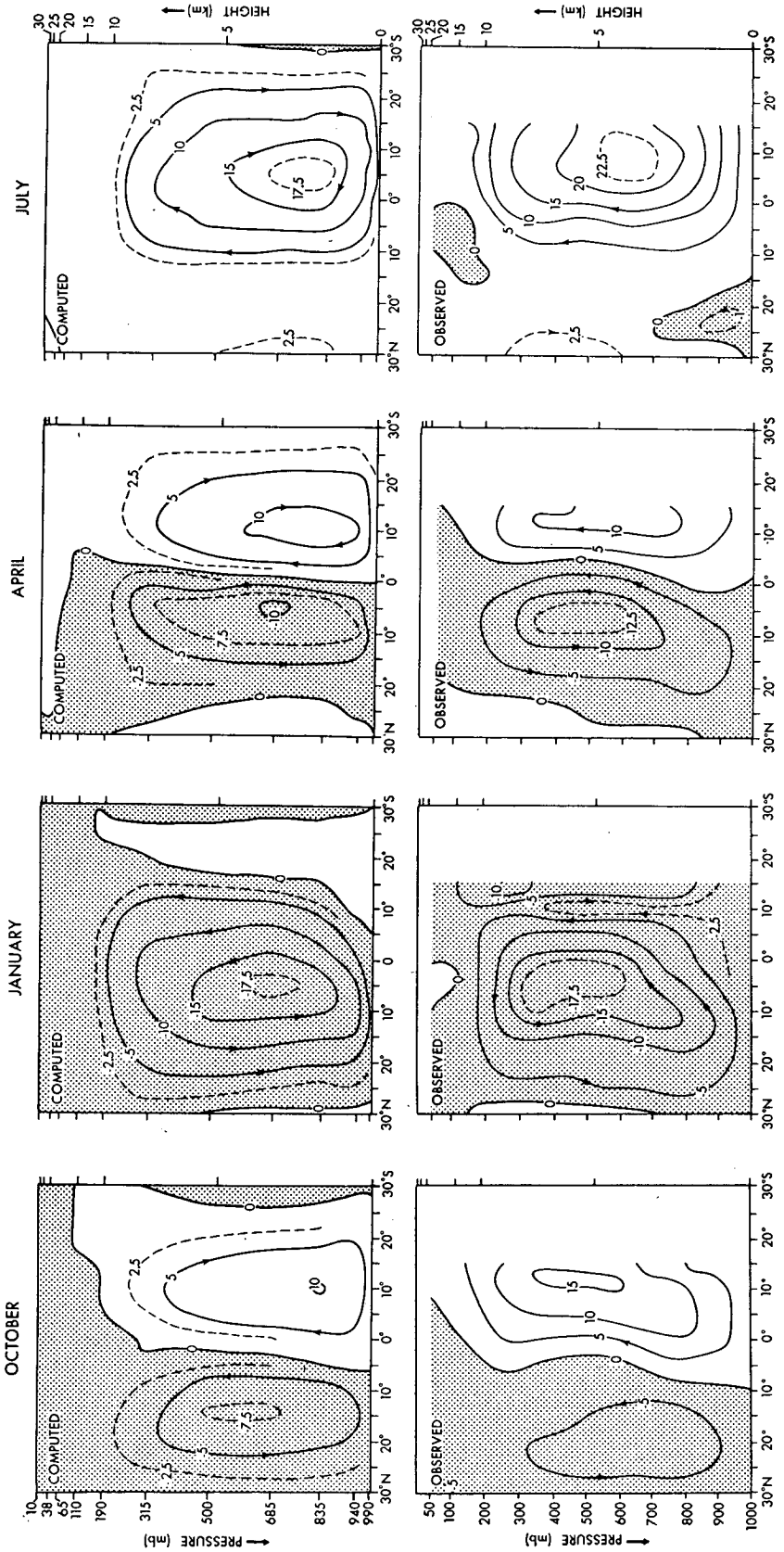

FIG. 3.4. Mean streamfunctions (10^{13} gm sec^{-1}) of the meridional circulation during October, January, April and July: upper half, computed; lower half, observed (Oort and Rasmusson, 1971).

b. Meridional circulation

The seasonal variation of the meridional circulation of the model tropics is illustrated in Fig. 3.4, which shows the streamfunction of meridional circulation in both the model and the actual atmospheres during four seasons of the year. According to this figure, the intensities of Hadley cells in both hemispheres of the model undergo a marked variation. In January, the northern cell practically occupies the entire model tropics and the southern cell is very weak and small. On the other hand, the former is very weak in July, and the latter dominates the tropics. Around October and April when the sun is located close to the equator, the intensities of the two cells are comparable. Comparing the seasonal variation of computed meridional circulation described above with that of the zonal wind shown in Fig. 3.2, one finds that intense easterly winds in the model tropics predominate where the meridional flow tends to be greatest. This relationship seems to be consistent with the law of conservation of absolute angular momentum. It is, however, necessary to examine the

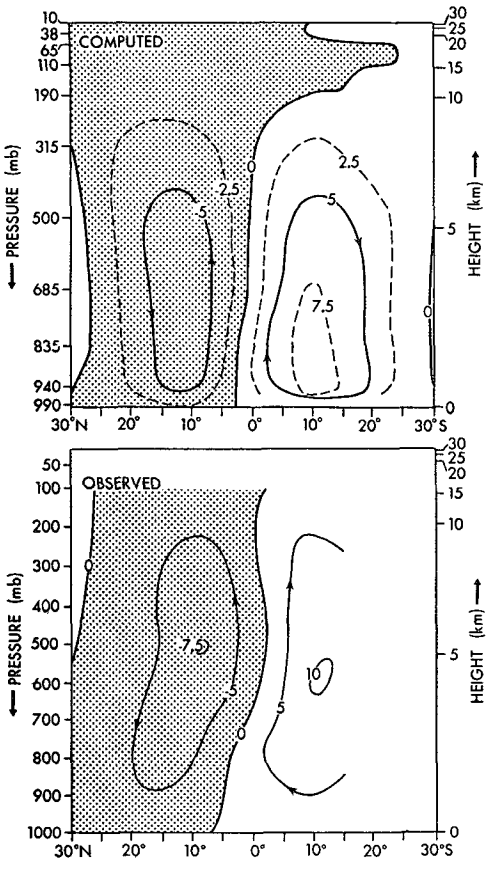

FIG. 3.5. Annual mean streamfunctions (10^{13} gm sec^{-1}) of the meridional circulation: upper half, computed; lower half, observed (Oort and Rasmusson, 1971).

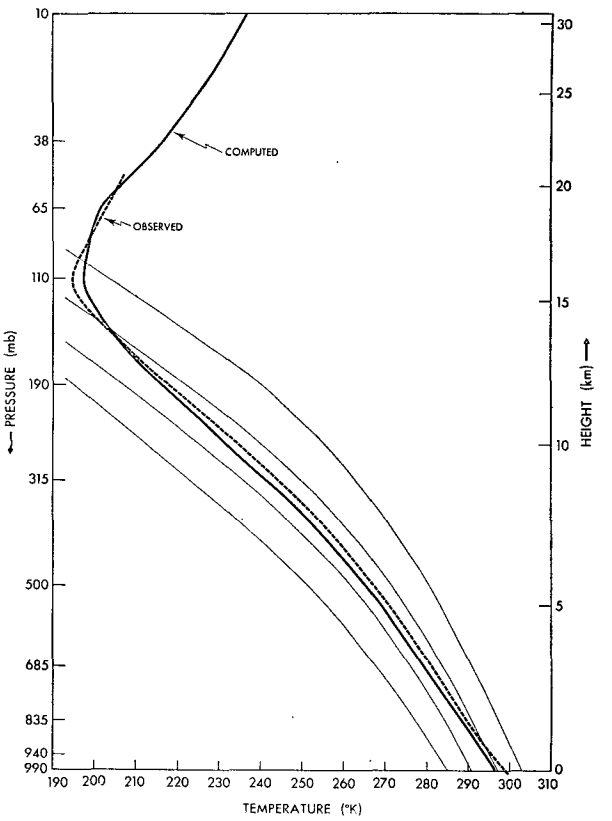

FIG. 3.6. Vertical distribution of temperature at the equator: solid line, computed; dashed line, observed (Oort and Rasmusson, 1971); thin solid lines, moist adiabats.

contribution of large-scale eddies to get a comprehensive picture of the budget of angular momentum. For further discussions of this subject, see Section 8.

The seasonal evolutions of the general features and the intensities of the two Hadley cells in the model tropics compare reasonably well with those in the actual tropics as obtained by Oort and Rasmusson (1971). There are, however, some systematic differences. The heights of the centers of the Hadley cells of the model are systematically lower than those in the actual tropics. It is highly probable that this discrepancy stems from the assumption of no subgrid-scale vertical mixing in the free atmosphere of the model. According to unpublished results from another numerical experiment by Manabe, the more extensive the layer of strong subgrid-scale vertical mixing, the higher the centers of the Hadley cells.

Finally, the annual mean streamfunctions of meridional circulation in the model tropics and in the actual tropics are shown in Fig. 3.5. Again the height of the center of the circulation is somewhat lower in the model atmosphere. The intensities of the two Hadley cells of the model are approximately 15% less than those of the actual atmosphere. The interface between the two Hadley cells in the model tropics is located slightly to

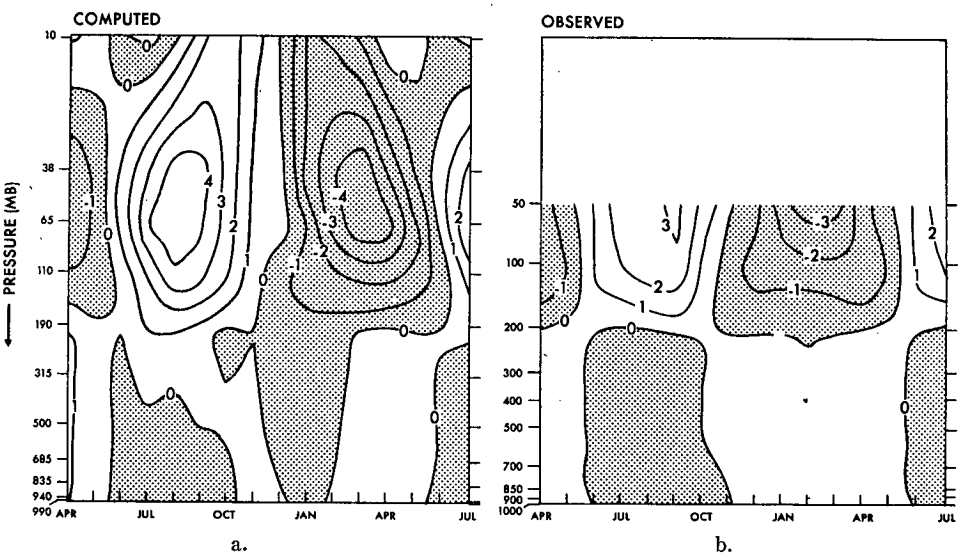

FIG. 3.7. Height-time distribution at the equator of temperature deviation (°K) from the annual mean: left, computed; right, observed (Oort and Rasmusson, 1971). In the observed graph, the last third of the figure is a repetition of the first part.

the north of the equator near the surface in qualitative agreement with the actual tropics.

c. Zonal mean temperature

The vertical distribution of the annual mean temperature at the equator of the model is compared with the corresponding distribution of the temperature of the actual tropics in Fig. 3.6. According to this comparison, the essential features of the thermal structure of the mean tropical atmosphere are successfully simulated by the model. For example, the equatorial tropopause of the model has an annual mean temperature of about −76C and its height is approximately 16 km. In the troposphere of the model, the static stability is super moist-adiabatic in the lower layers and sub moist-adiabatic in the upper layers. These features of the thermal structure of the model tropics are in excellent agreement with those of the actual tropics. However, further examination of the results reveals that the static stability is too stable in the upper troposphere. It is probable that this discrepancy results from the idealization involved in the process of convective adjustment.

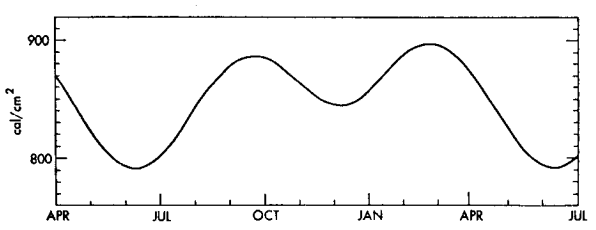

FIG. 3.8. Seasonal variation of insolation (cal cm^{-2} day^{-1}) at the equator.

Fig. 3.7a shows the seasonal variation of temperature deviation from the annual mean at the equator of the model. According to this figure, temperatures undergo a maximum seasonal variation in the lower stratosphere i.e., around 30–100 mb. Temperature reaches its maximum in about August and its minimum during March. These features of temperature variation in the model atmosphere agree qualitatively with those of observed temperature variation shown in Fig. 3.7b. The variation of temperature described here has little resemblance to the seasonal variation of insolation at the equator shown in Fig. 3.8.[2] This result indicates a strong dynamical control over temperature in the lower stratosphere (see Reed and Vleck, 1969). However, the temperature variation at the 10-mb level of the model has some resemblance to the variation of insolation, suggesting an increase in the relative importance of the effect of the absorption of solar radiation with increasing altitude. The seasonal variations of temperature and heat balance in the stratosphere of the model tropics will be discussed further in a companion paper by Manabe *et al.* (1974). Finally, it should be pointed out that the amplitude of the seasonal variation in the troposphere of the model is relatively small.

4. Precipitation

The horizontal distribution of the annual mean rate of precipitation of the model is compared with the observed distribution in Fig. 4.1. According to this figure, the major center of intense rainfall of the model occupies the western Pacific and Indian Oceans. A

[2] The minimum in insolation at the December solstice is greater than that at the June solstice because the sun is 3% closer to the Earth then.

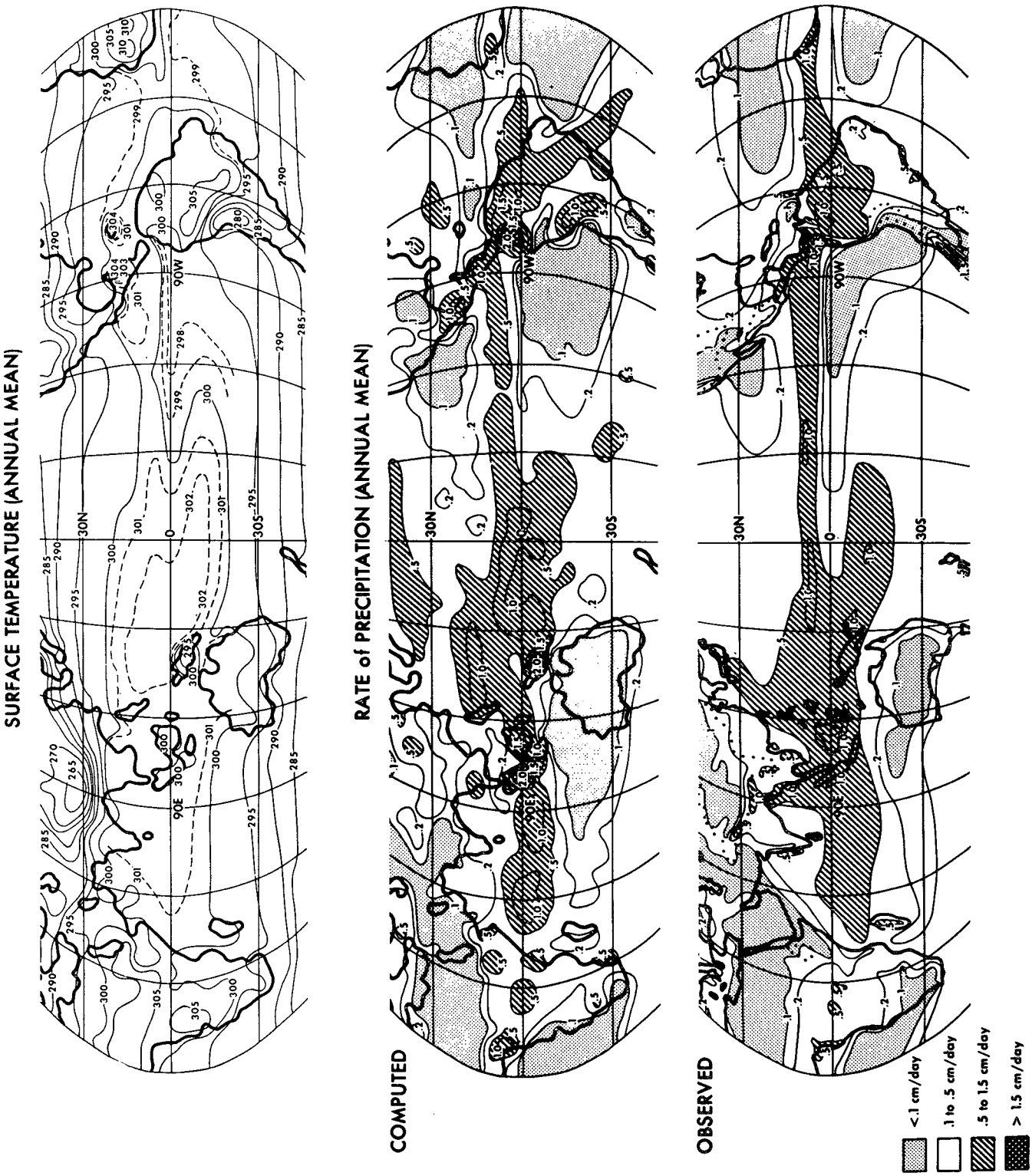

FIG. 4.1. Top, annual mean temperature (°K) at the earth's surface of the model; middle, computed annual mean rate of precipitation (cm day^{-1}); bottom, observed (USSR Academy of Sciences, 1964) annual mean rate of precipitation (cm day^{-1}).

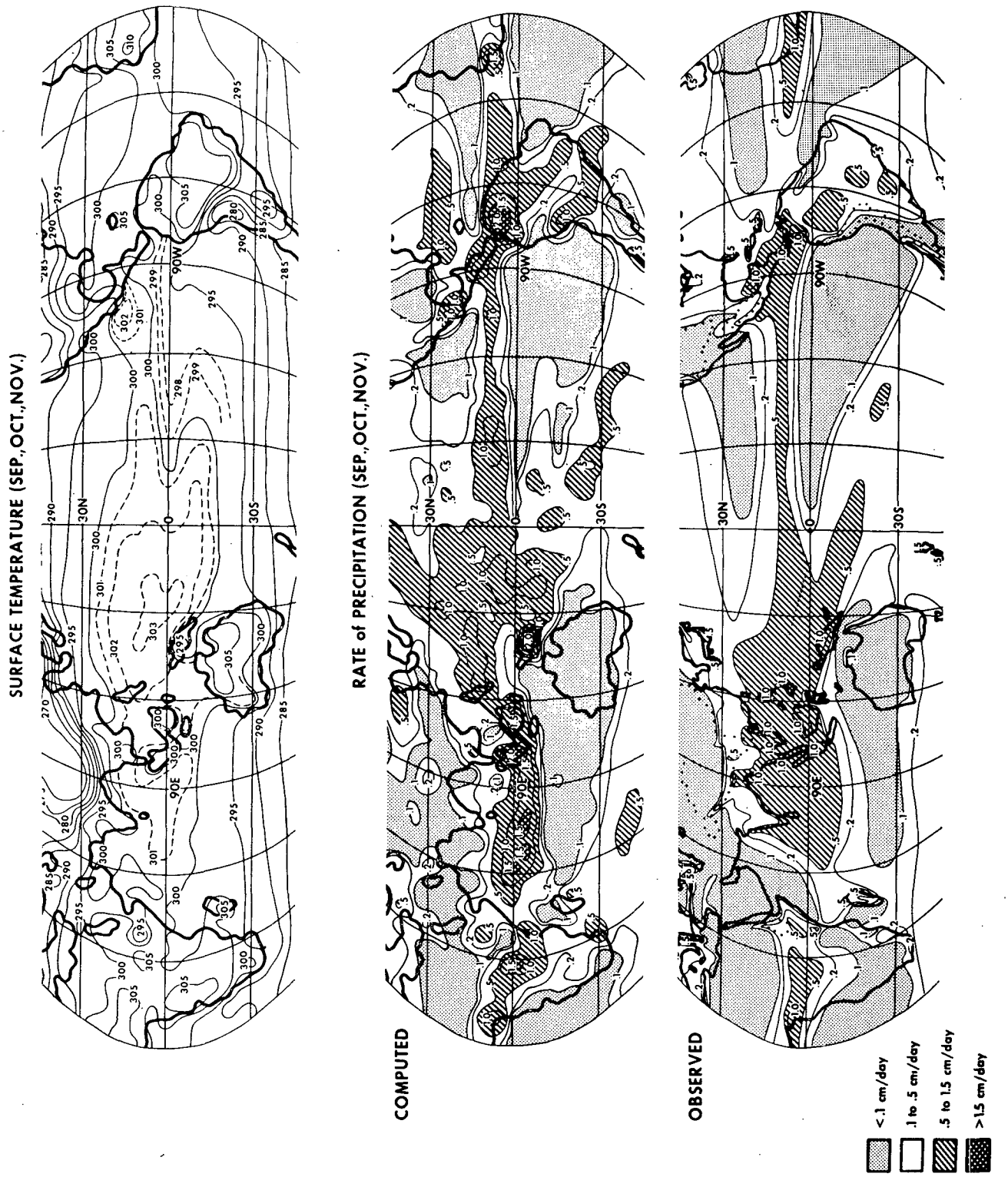

FIG. 4.2a. Top, 3-month mean temperature (°K) at the earth's surface of the model; middle, computed 3-month mean (Sept., Oct., Nov.) rate of precipitation (cm day^{-1}); bottom, observed (Möller, 1951) 3-month mean rate of precipitation (cm day^{-1}). All values based on period September–November.

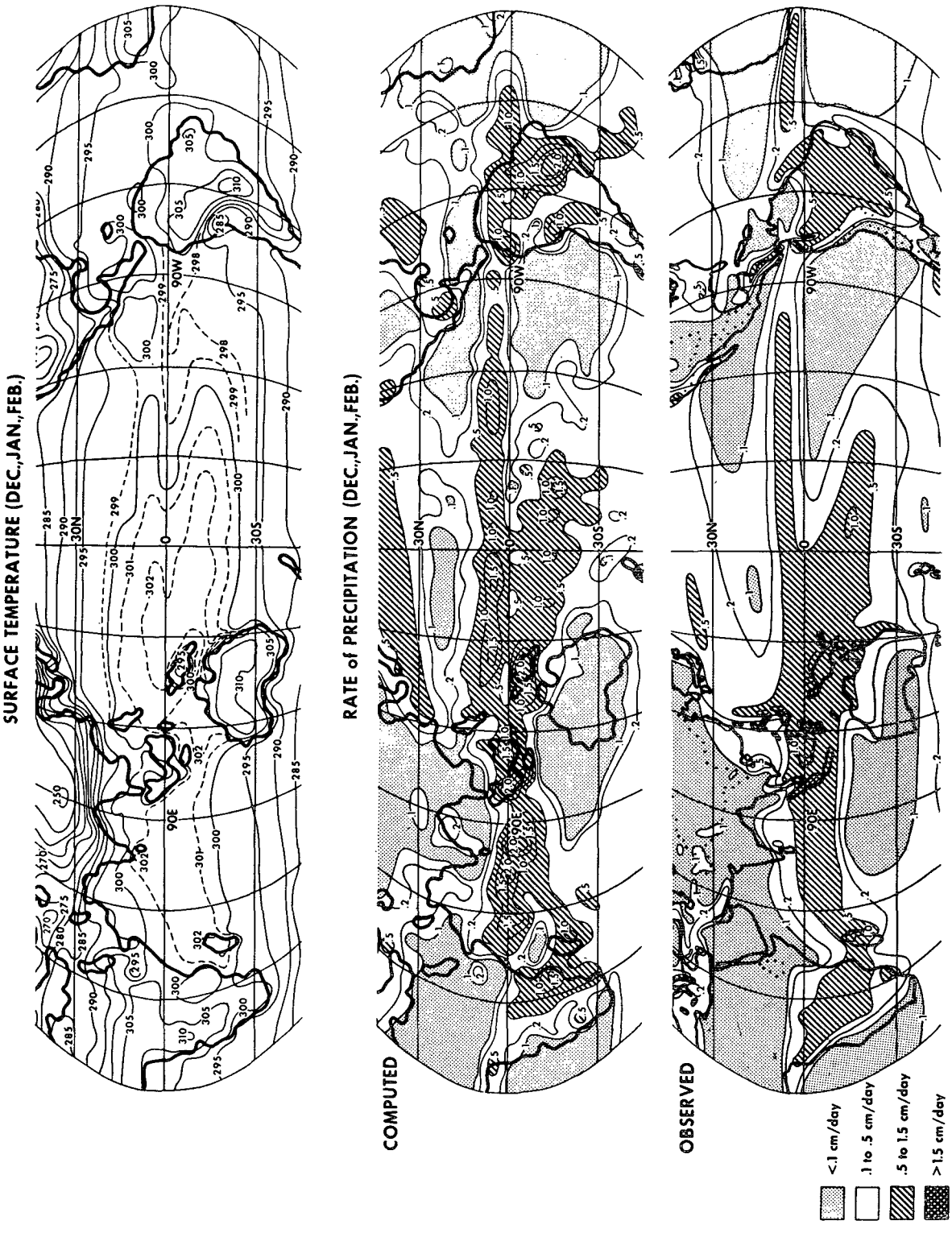

Fig. 4.2b. As in Fig. 4.2a except for December–February means.

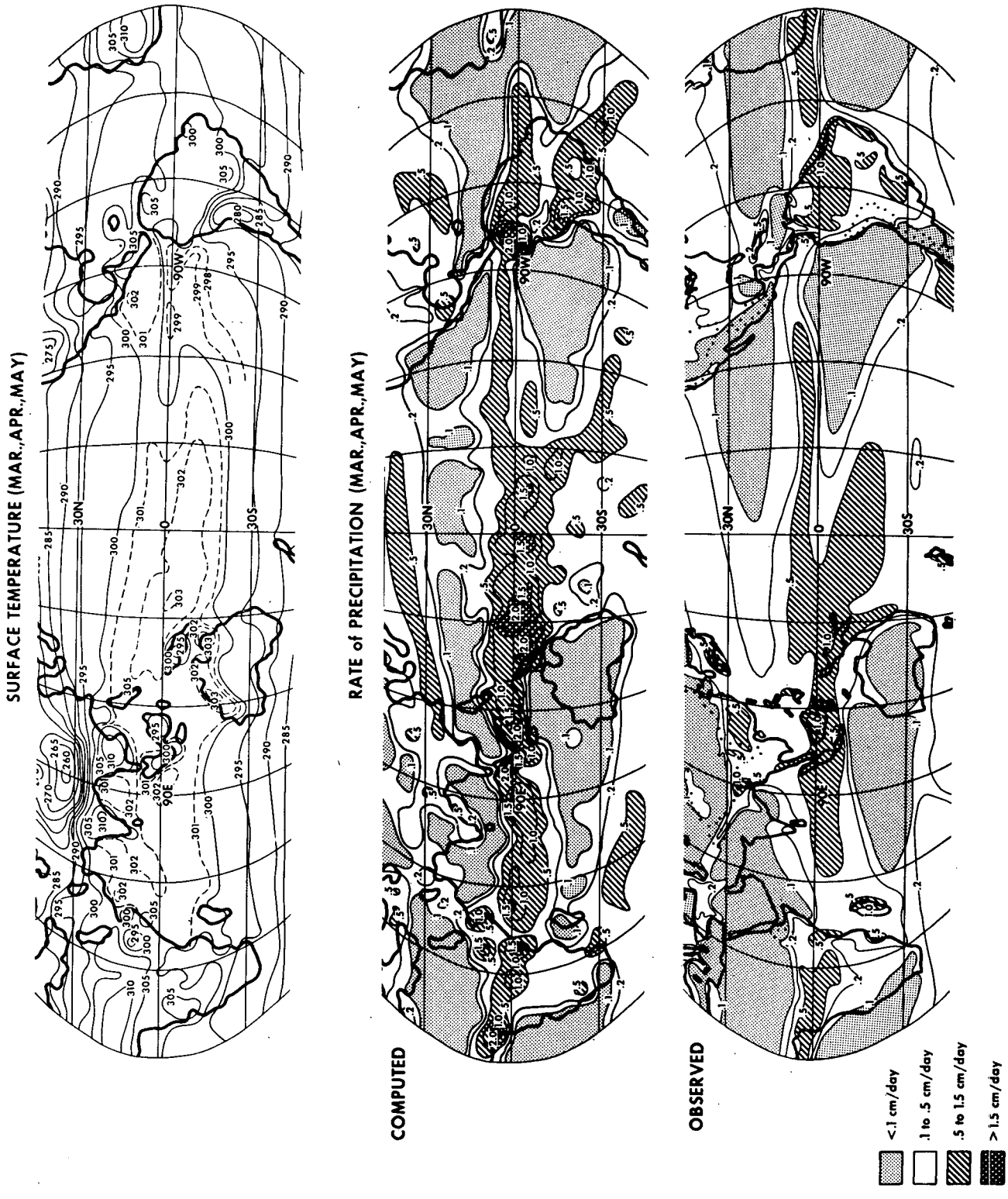

FIG. 4.2c. As in Fig. 4.2a except for March–May means.

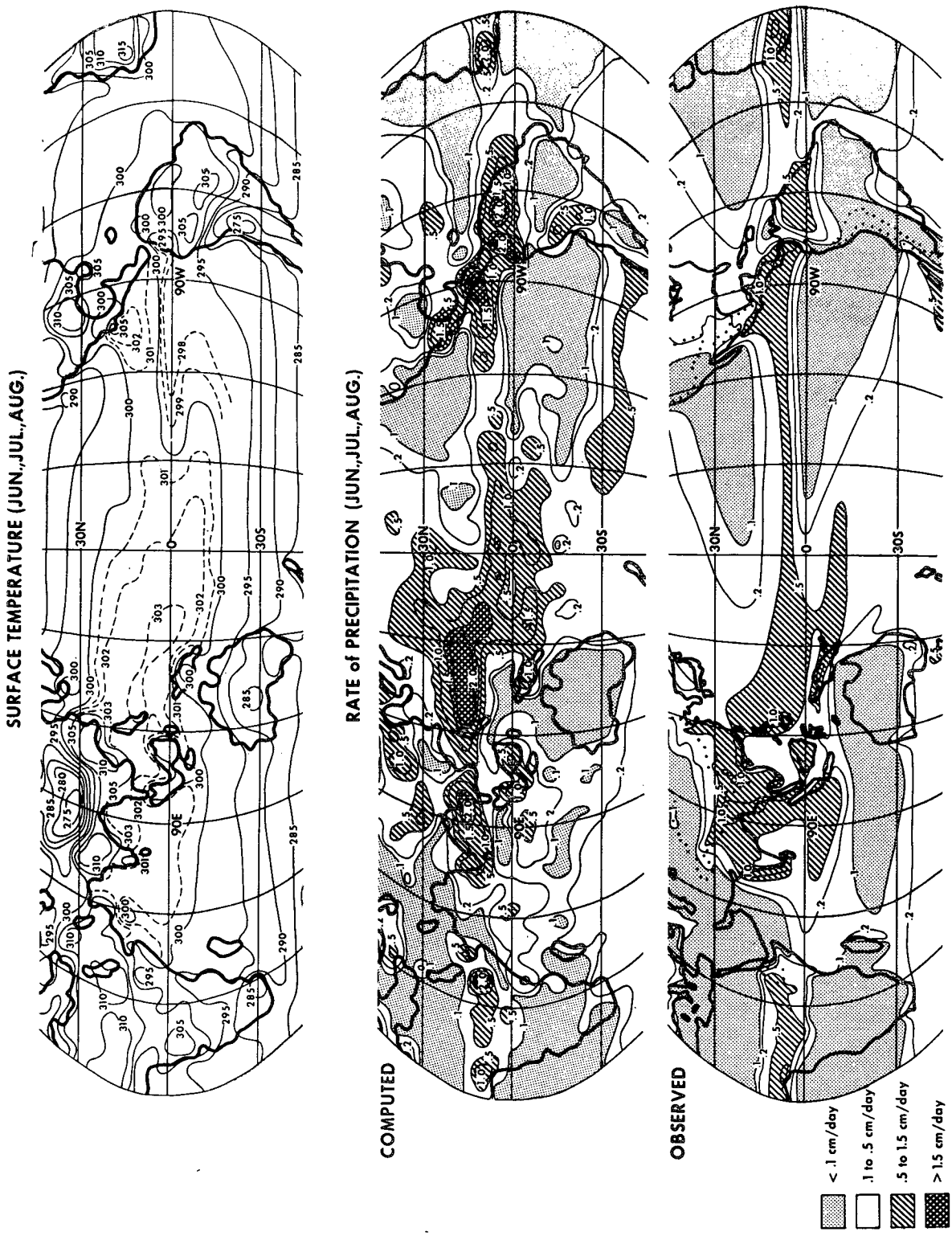

FIG. 4.2d. As in Fig. 4.2a except for June–August means.

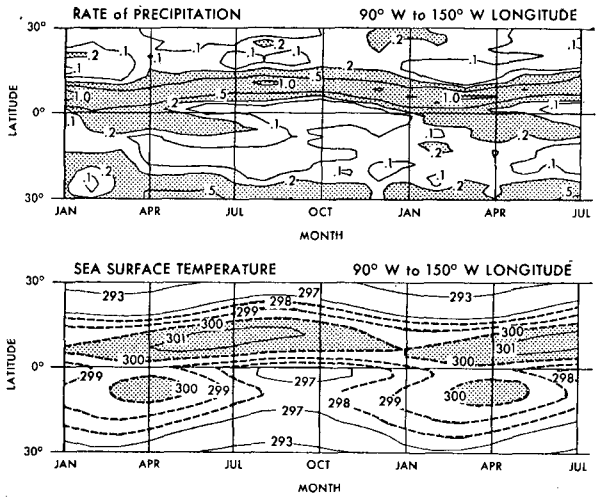

FIG. 4.3. Latitude-time distributions in the eastern Pacific: top, zonal mean rate of precipitation (cm day^{-1}); bottom, zonal mean sea surface temperature (°K). The zonal means represent an average over the longitudinal range from 90 to 150W.

secondary center is located in the general area of the Amazon River basin. In the eastern Pacific of the model, the northern branch of the tropical rainbelt is located just north of the equator. The southern branch originates from the central Pacific and extends towards the southern end of South America. These features of the simulated tropical rainbelt are in excellent agreement with those of the observed tropical rainbelt. If one compares the patterns of annual mean rainfall of the model with the distribution of the annual mean sea surface temperature, also in Fig. 4.1, one finds excellent correspondence between the two. For example, the area of intense precipitation in the western Pacific and Indian Oceans of the model coincides very well with an area of high sea surface temperatures. Furthermore, the tropical rainbelt located in the eastern Pacific of the model coincides with a belt of warm sea surface temperatures parallel to the equator. This correspondence suggests that the tropical rainbelt tends to be located over regions of warm sea surface temperatures.

The distributions of the rate of precipitation of the model averaged over four quarter-year periods are given in Figs. 4.2a–d. The tropical rainbelts over Africa and South America of the model undergo a large latitudinal translation from season to season. They are furthest south in the December–February period and furthest north in June–August. Over the oceans of the model, the amplitude of the seasonal movement of the rainbelt is less and seems to be strongly related to the seasonal movement of the area of relatively warm sea surface temperatures (see the top part of Figs. 4.2a–d). For example, the area of intense precipitation in the western Pacific of the model extends northward in June–August and later retreats toward the equator following closely a similar change in the area of maximum sea surface temperatures. In general, the above described simulated precipitation distributions for the four seasons agree well with the observed precipitation distributions which are shown in the bottom parts of Figs. 4.2 a–d.

Satellite observations of cloud cover show the tendency of the tropical rainbelt to form away from the equator over tropical oceans. For example, Bjerknes *et al.* (1969) show a satellite picture of the monthly mean brightness in April and note the existence of two bright belts on both sides of the equator in the eastern Pacific. They suggest that the location of the ITCZ is essentially controlled by the distribution of sea surface temperatures and that the equatorial belt of cold sea surface temperatures, which results from the upwelling of water, prevents the ITCZ from forming at the equator. On the other hand, Charney (1966) and Bates (1970) suggest, on the basis of results from theoretical as well as numerical studies, that the ITCZ has an inherent tendency to avoid the equator. Therefore, it is desirable to examine the results of this model experiment in this respect. In Fig. 4.3, the latitude-time distribution of the zonal mean rate of precipitation and that of the zonal mean sea surface temperature in the eastern Pacific of the model are contrasted with each other. The zonal means are computed over the longitudinal sector ranging from 90 to 150W. According to this figure, the tropical rainbelt of the eastern Pacific

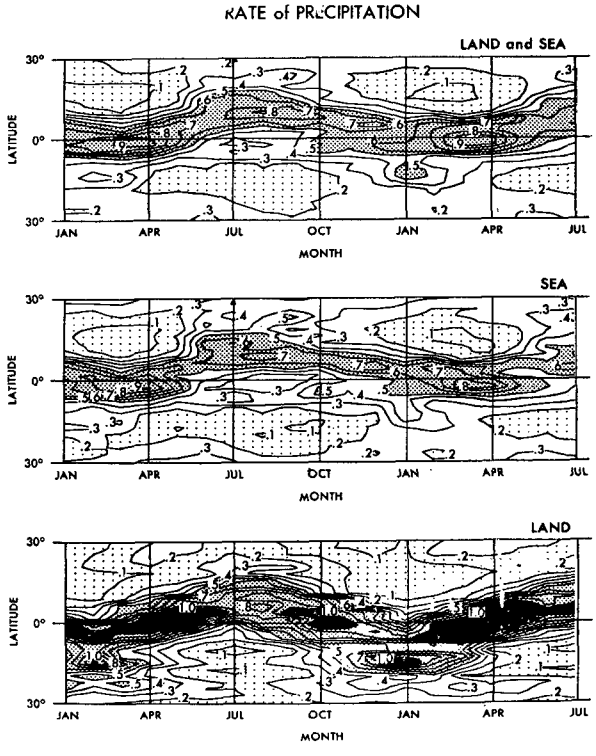

FIG. 4.4. Latitude-time distributions of the zonal mean rate of precipitation of the model (cm day^{-1}): top, zonal mean over both continents and oceans; middle, zonal mean over oceanic regions; bottom, zonal mean over continental regions.

in the model remains in the Northern Hemisphere throughout the year with the warmer sea surface temperatures. A secondary rainbelt forms just south of the equator around April when a secondary maximum of sea surface temperatures appears in the Southern Hemisphere. The monthly charts of brightness, compiled by Taylor and Winston (1968), indicate that the double ITCZ of the eastern Pacific, as observed by satellites, is most pronounced around April in qualitative agreement with the features of the model atmosphere.

Fig. 4.3 indicates that the rate of rainfall at the equator of the model is very small around October. Again, this minimum corresponds well with the minimum in sea surface temperatures, which becomes notable around October due to intensified upwelling at the equator. These results indicate the strong control the sea surface temperatures exert upon the location of the ITCZ. Therefore, it is not possible to prove that the double precipitation maxima are evidence of an inherent tendency of the ITCZ to avoid the equator. According to Fig. 4.4, which shows the seasonal variation of the zonal mean rate of precipitation averaged over the continental and the oceanic regions separately, the tropical rainbelt of the model has no tendency to avoid the equator over the continents. Although precipitation tends to be smallest as the rainbelt crosses the equator over the oceanic regions, it is greatest exactly at the equator over the continental regions where an equatorial minimum of surface temperatures does not exist. This result suggests that the tropical rainbelt of the model does not necessarily have a tendency to avoid the equator.

In order to explore this problem further, it is desirable to carry out a numerical integration of the general circulation model with and without the equatorial belt of cold sea surface temperatures and to try to determine how various factors such as sea surface temperature and the Coriolis parameter control the location of the ITCZ. Although such studies have not yet been done, we found results from an earlier numerical experiment useful in gaining some insight into this matter.

Recently, Holloway and Manabe (1971) performed a numerical time integration of a model, which is very similar to the present model, by assuming the field distributions of insolation and sea surface temperatures for January. The distribution of sea surface temperature adopted for this experiment was taken from the old publication of the Hydrographic Office (1944). Fig. 4.5 shows the horizontal distributions of precipitation rates and sea surface temperatures of their model.

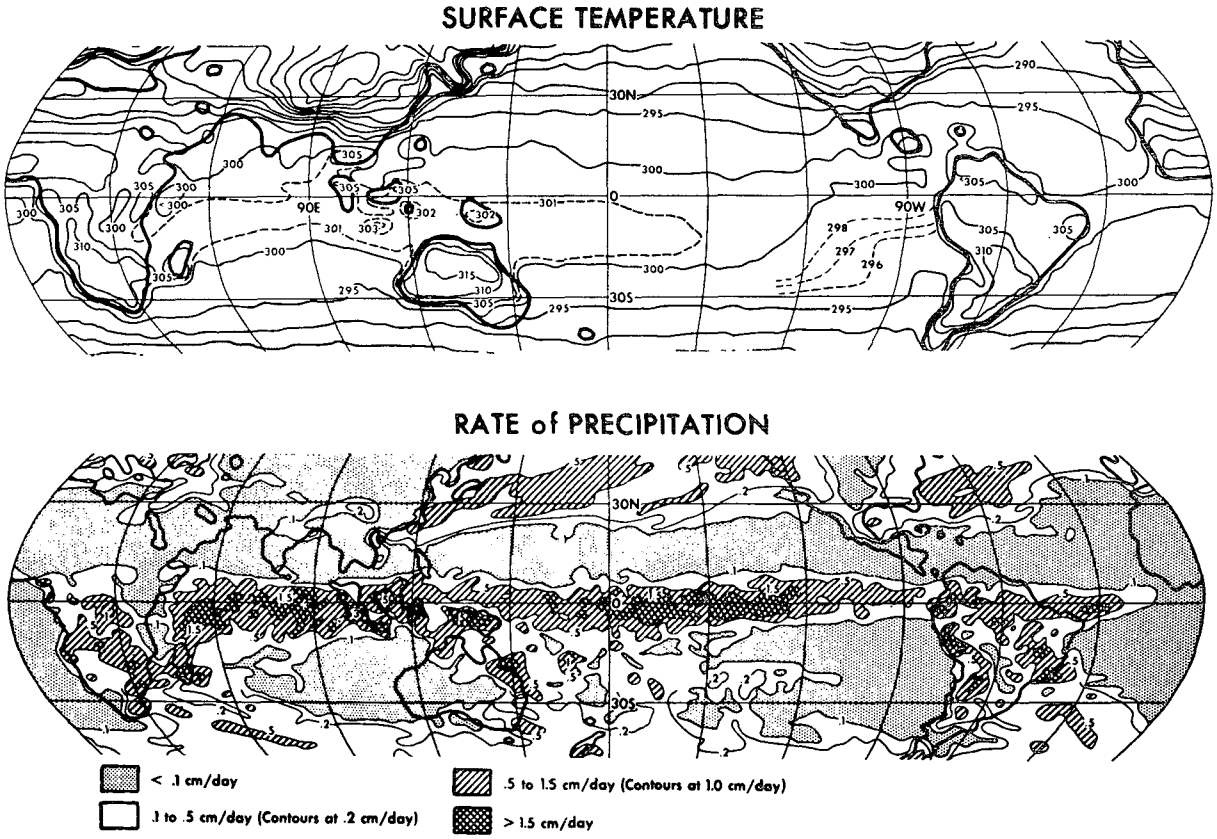

FIG. 4.5. Results from the high-resolution model of Holloway and Manabe (1971): top, horizontal distribution of surface temperature (°K); bottom, the rate of precipitation (cm day^{-1}).

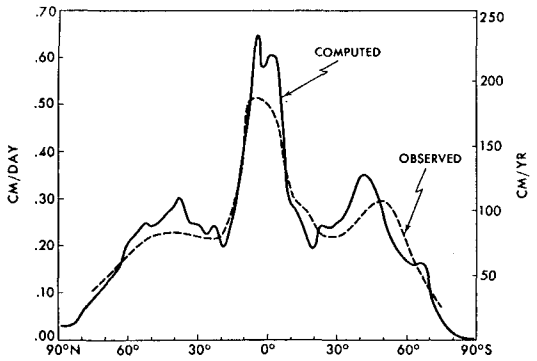

FIG. 4.6. Latitudinal distributions of the yearly-averaged, zonal mean rate of precipitation: solid line, computed; dashed line, observed (Budyko, 1956).

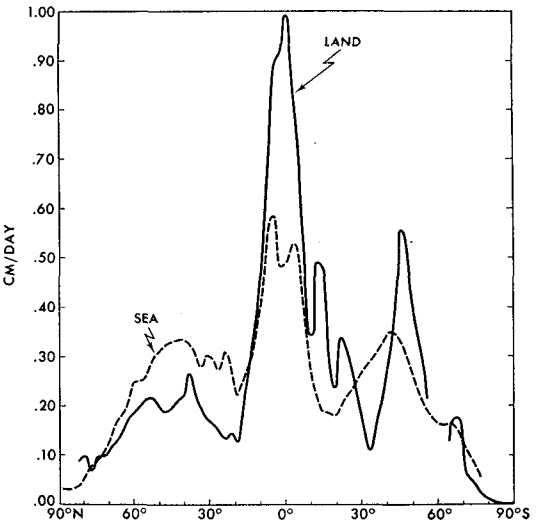

FIG. 4.7. Latitudinal distributions of the yearly-averaged, zonal mean rate of precipitation: solid line, zonal means over continental regions; dashed line, zonal means over oceanic regions.

This figure indicates that the distribution of sea surface temperatures adopted for their study is quite different from that of this study, particularly in the eastern Pacific. For example, their distribution does not reflect the distinct equatorial belt of cold sea surface temperatures, and the areas of maximum sea surface temperature are much less pronounced than in the present version. In response to this distribution, the rainbelt of the model forms directly on or very close to the equator. This result seems to suggest that the tropical rainbelt of the model has a inherent tendency to form at the equator unless it is discouraged by relatively cold sea surface temperatures at the equator. A similar tendency was also noted in a numerical experiment by Manabe (1969a).

In summary, the results described here do not agree with those of Charney (1966) and Bates (1970). Pike (1971) pointed out that the ITCZ in the Bates model should form away from the equator under any circumstances because of the assumption of no boundary layer pumping of moisture at the equator (see also Bates, 1971). In his theoretical study, Charney assumes that the ITCZ is zonal and symmetric relative to the equator. As is discussed toward the end of this section, the tropical rainbelt of the model consists of chains of cells of intense precipitation. Therefore, further refinement of these theoretical studies as well as further improvements in the computational resolution of the model are required before settling this question.

In order to evaluate quantitatively the rate of precipitation of the model in relation to the observed rate of precipitation, the annual mean rate of precipitation of the model is shown in Fig. 4.6 as a function of latitude and is compared with the distribution of the actual precipitation rate estimated by Budyko (1956). The agreement between the two distributions is reasonably good except that the precipitation rate in the tropics is overestimated by the model. However, the difference between the observed and computed rates may not be larger than the magnitude of the ambiguity in estimating the rate of tropical rainfall. Fig. 4.7 shows the

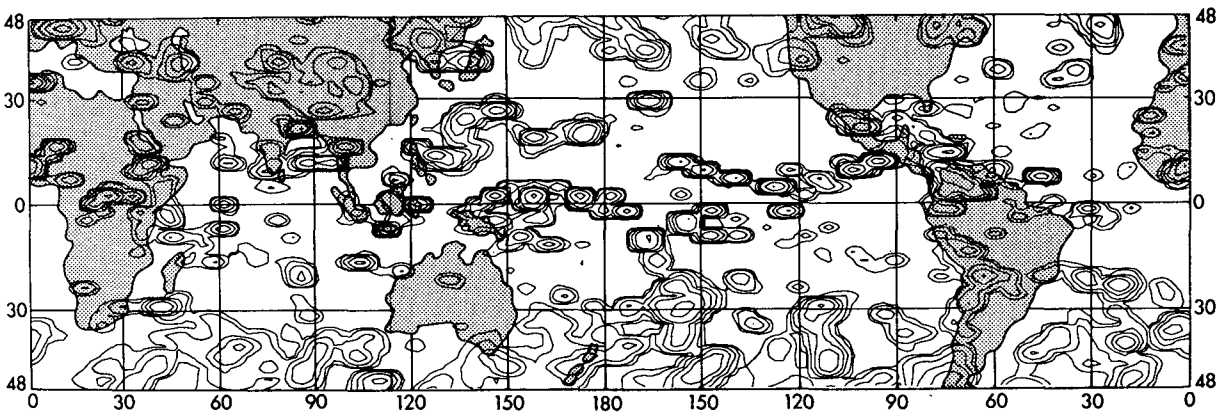

FIG. 4.8. Horizontal distribution of the 6-hr mean rate of precipitation on 14 July in the model. Contours: 0.1, 0.2, 0.5, 1.0, 2.0, 5.0, 10.0, 20.0 cm day^{-1}.

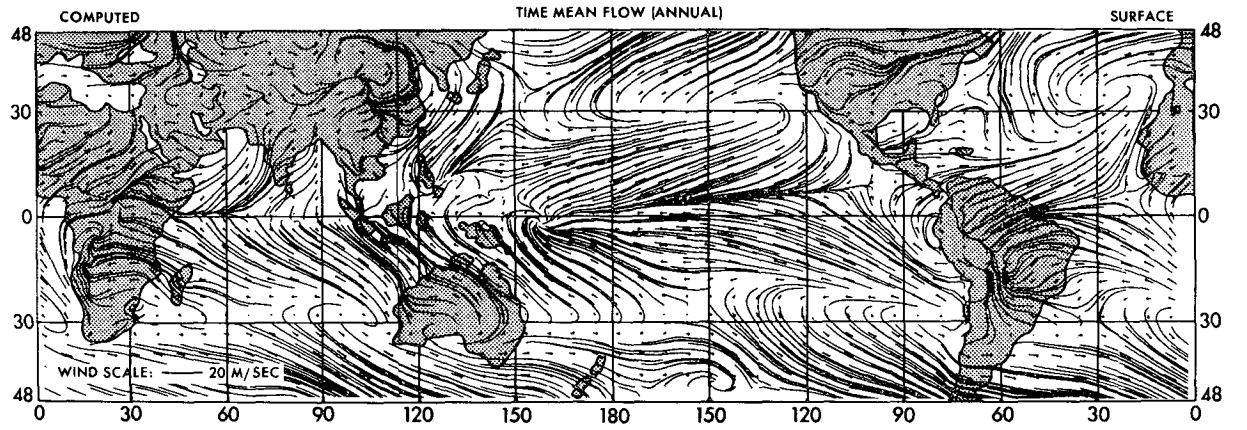

FIG. 5.1. Annual mean vectors and streamlines near the earth's surface ($\sigma = p/p_* = 0.99$) of the model. The length of the vector is proportional to the wind speed. The length of a 20 m sec^{-1} vector is shown in the lower left-hand corner of the map.

latitudinal distributions of the rates of precipitation over the continents and the oceans separately. Over the oceanic regions, the rate of precipitation has a weak local minimum at the equator owing to the contribution from the oceanic region where sea surface temperature has a local minimum. Over the continental regions, it is greatest directly on the equator.

The distributions of the rate of precipitation discussed so far represent averages taken over long periods of time. In order to show how precipitation averaged over a short period of time is distributed, a map of 6-hr mean precipitation rate is reproduced in Fig. 4.8. This figure indicates that the tropical rainbelt is not a quasi-two-dimensional belt of heavy rainfall but consists of a chain of many cells of rainfall. This feature of the tropical rainbelt was noted by Malkus (1962). As pointed out in the introduction, Manabe and Smagorinsky (1967), Manabe (1969) and Bates (1970) obtained tropical rainbelts with similar cellular structures. It is probable that these synoptic-scale cells of precipitation correspond to the cloud clusters which are visible in satellite pictures of the tropics. In the model tropics, these centers of precipitation are often accompanied by synoptic-scale disturbances as already shown by Manabe and Smagorinsky (1967) and Manabe *et al.* (1970). For example, Hayashi (1973) found transient disturbances with periods of 5 days and with wavenumbers of about 10 in the narrow tropical rainbelt located in the eastern Pacific of this model.

5. Streamlines

a. Lower troposphere

Surface streamlines computed from the model's annual mean wind field (at level 11 where $p/p_* = 0.99$) are shown in Fig. 5.1. This map is characterized by the divergence from the oceanic anticyclones in the subtropics and the convergence into a narrow belt near the equator, i.e., the intertropical convergence zone (ITCZ). Over the eastern Pacific and the eastern Atlantic, the ITCZ of the model is located several degrees of latitude to the north of the equator, whereas it is located very close to the equator over the western Atlantic, part of the western Pacific, and over the Indian Ocean. Over continental regions, the convergence zones spread widely in the meridional direction, which is probably related to a large seasonal variation of temperature over land surfaces. In general, the location of the ITCZ of the model coincides well with the location of the tropical rainbelt, except over Africa, where the ITCZ is located slightly to the north of the tropical rainbelt.

The seasonal variation of flow field near the earth's surface of the model is illustrated in Fig. 5.2, which shows streamlines computed from one-month mean wind fields for four months of the year. One of the most striking features of these distributions is the intense cross-equatorial, southerly wind over the Indian Ocean and the western side of the Pacific in July. The southerly wind accounts for most of the mass transport by the cross-equatorial Hadley cell in July and supplies large amounts of moisture to the monsoon rainbelt over India and Indochina. In January, the direction of surface flow is opposite in the northern Indian Ocean. The northerly wind blowing out of the Siberian high reaches the equator and forms the ITCZ slightly to the south of the equator. The features of the surface flow described above are in excellent agreement with those in the actual atmosphere shown in Fig. 5.3.

In the western Pacific of the model, a pronounced trough, oriented from southwest to northeast, develops in July along the coast of the Eurasian continent. According to Sadler,[3] such a trough does become established in the actual atmosphere for periods of about a week but does not appear in the monthly mean map. This unrealistic feature reflects the excessive development of tropical cyclones in the western Pacific of the model.

[3] Private communication.

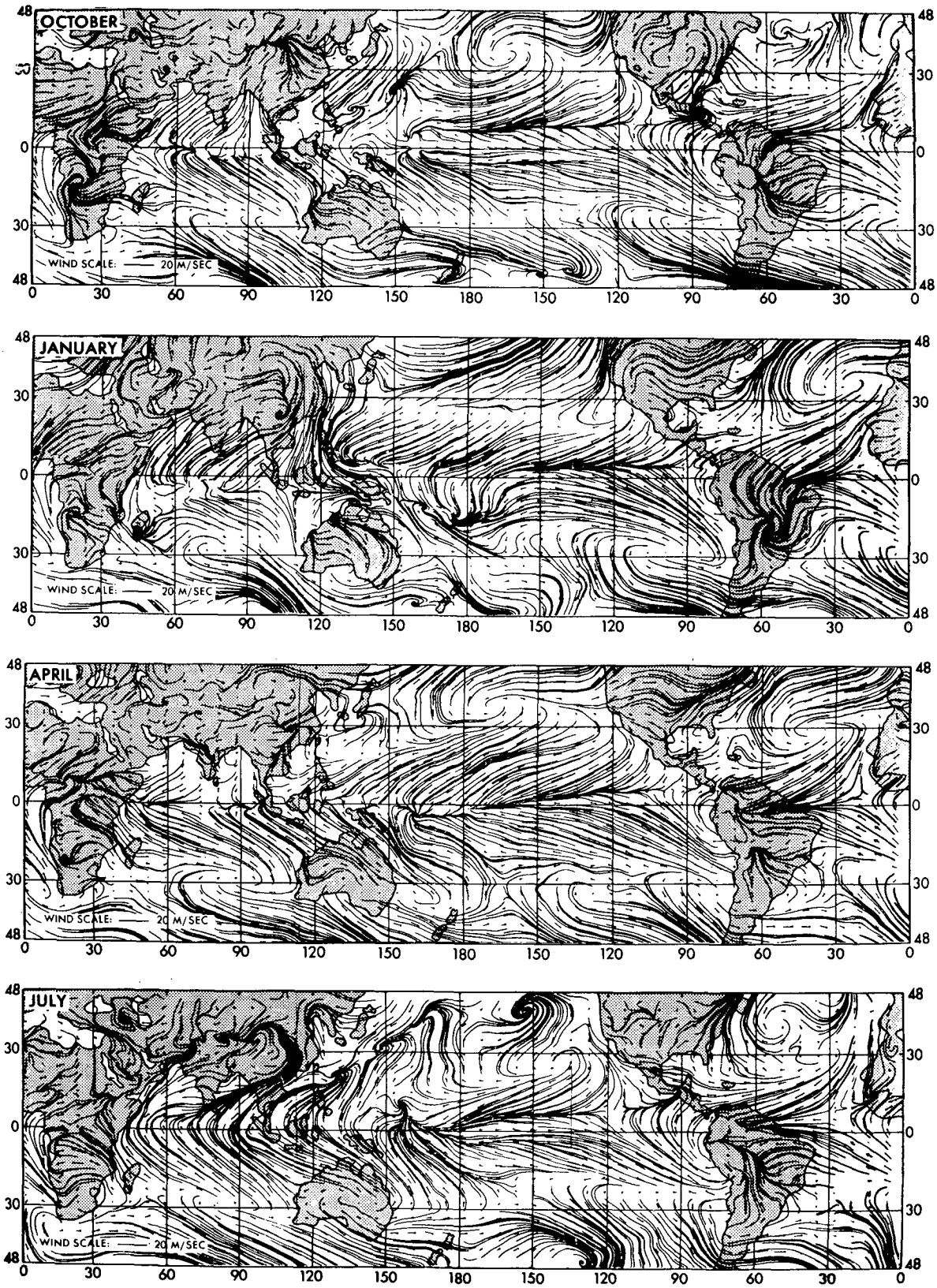

FIG. 5.2. One-month mean vectors and streamlines near the earth's surface ($\sigma = p/p_* = 0.99$) of the model during October, January, April and July. The length of the vectors is proportional to the wind speed. The length of a 20 m sec^{-1} vector is shown in the lower left-hand corner of each map.

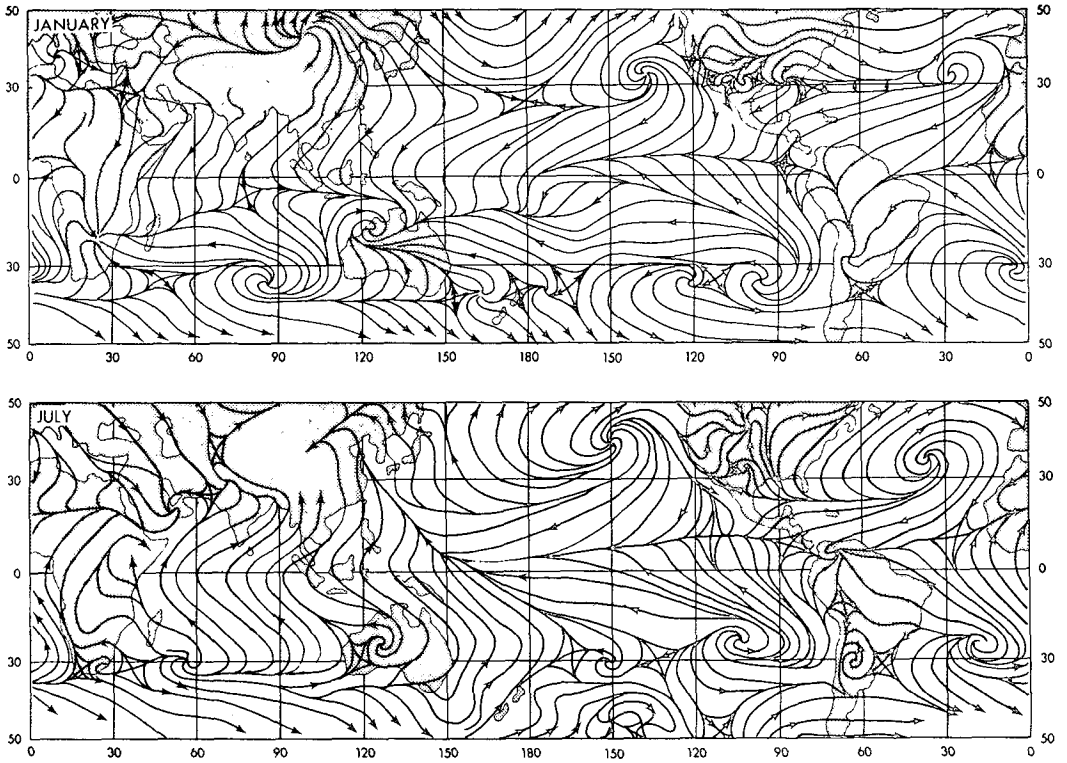

FIG. 5.3. Observed 1-month mean streamlines at the earth's surface during January (Mintz, 1968) and July (Mintz, 1952).

In the eastern Pacific of the model, the ITCZ is located to the north of the equator throughout the year. It is located furthest north around August and September and furthest south around February and March. The movement of the ITCZ described here corresponds very well with that of the tropical rainbelt of the model discussed in the preceding section. Over the Atlantic, the ITCZ undergoes a similar movement with respect to season. However, it approaches very close to the equator around the January–April period as a result of the lack of an equatorial belt of cold water. Again, the seasonal movement of the ITCZ in the eastern Pacific and the Atlantic of the model compares well with that in the actual atmosphere (Fig. 5.3).

Over the continental regions of the model, the ITCZ undergoes large seasonal movements and does not always line up in the zonal direction. For example, warm moist air over a wide area of the Atlantic Ocean converges into the South American continent and forms the ITCZ at various latitudes. As Fig. 5.2 indicates, the ITCZ over South America extends to 25S in January and shifts back to the equatorial region around July. Over the African continent, one can also see a wide latitudinal movement of convergence zones with respect to season. Again, the convergence zone reaches furthest south around January. In general, the seasonal variation of the convergence zones over the model continents corresponds well with that of the tropical rainbelt discussed in the preceding section. However, it is noteworthy that the location of the ITCZ over western Africa does not agree exactly with that of the tropical rainbelt. In more specific terms, the ITCZ is always located to the north of the rainbelt. The contrast between the northeasterly wind from the Sahara with very low relative humidity and the humid southwesterly wind (southwest monsoon) may explain the reason for the different locations of the ITCZ and the tropical rainbelt in western Africa.

b. Upper troposphere

The flow field in the upper troposphere of the model tropics is quite different from that near the earth's surface. This is evident in Fig. 5.4, which includes the annual mean streamlines at the 190-mb level. One of the most outstanding features of the upper troposphere flow are the pairs of anticyclonic vortices which straddle the equator. For example, a pair of large anticyclonic vortices is located over the western Pacific on both sides of the equator. Over Central America, less distinct but similar features are evident, i.e., streamlines with anticyclonic curvecture lie on both sides of the equator. To the east of these anticyclonic pairs, very intense equatorial westerlies predominate over the eastern Pacific and Atlantic Oceans. One can also identify so-called mid-oceanic troughs on both sides of the

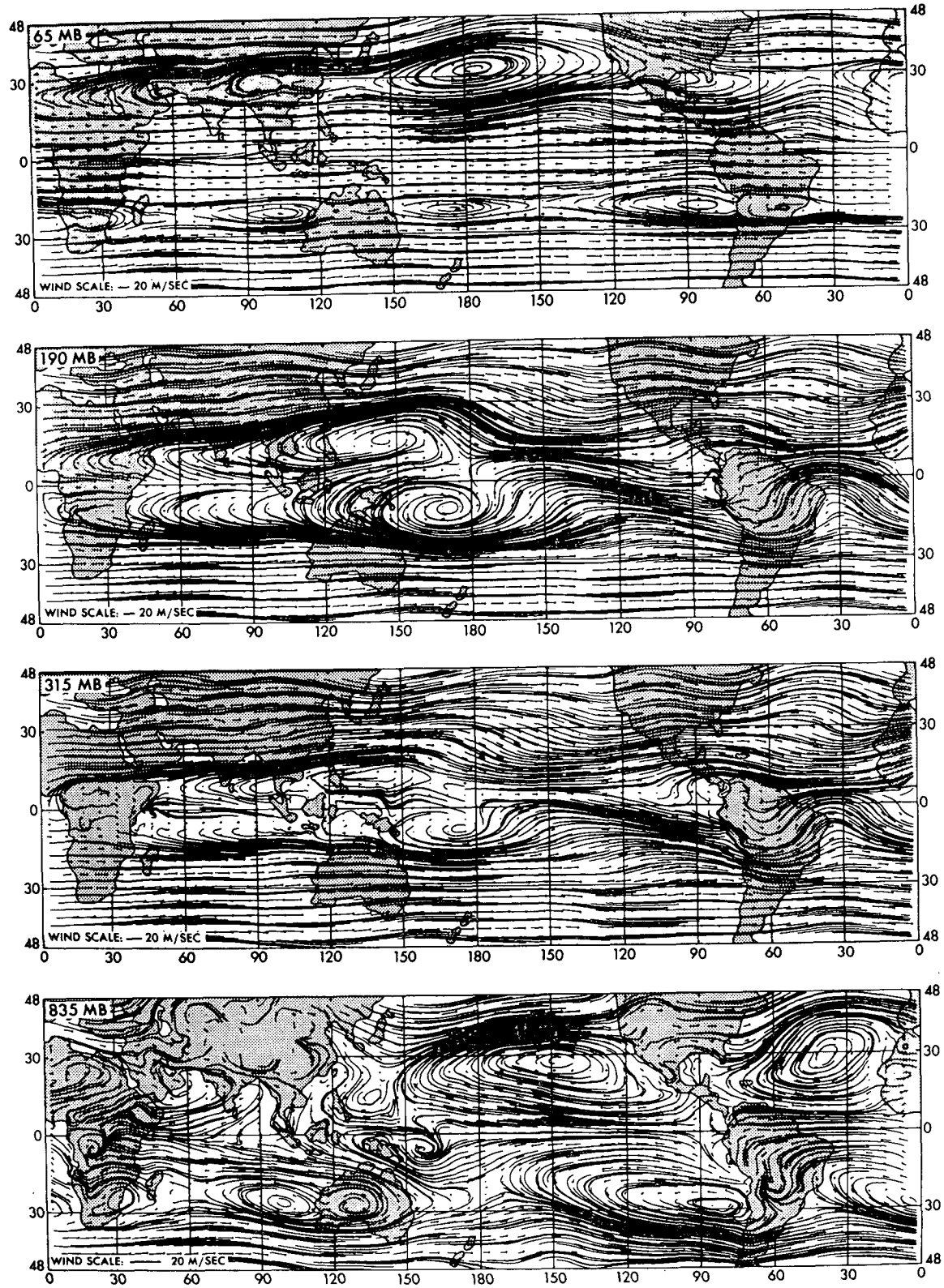

FIG. 5.4. Annual mean vectors and streamlines at the 65-, 190-, 315- and 835-mb levels of the model atmosphere. The length of the wind vectors is proportional to the wind speed. The length of a 20 m sec^{-1} vector is shown in the lower left-hand corner of each map. Note that the scale for the wind vectors varies from one level to another.

equator in the eastern Pacific and the Atlantic. The basic features of the upper tropospheric flow described above seem to be consistent with the theories of Matsuno (1966b) and Webster (1972) on the stationary disturbances in the tropics. Using a simple barotropic model, Matsuno demonstrated that mass sources and sinks introduced alternatively along the equator can create intense flows from the sources to the sink. His theory also calls for pairs of anticyclonic vortices straddling the equator near the mass sources and pairs of cyclonic vortices near the mass sinks. According to his analysis, the mass source or sink in his barotropic model may be interpreted as a heat source or sink in a three-dimensional model of the atmosphere. Therefore, one can speculate that the two pairs of anticyclonic vortices, the mid-oceanic troughs and the equatorial westerlies, which appear in the upper troposphere of the model, result from the great amount of heat released by condensation over the western Pacific and Central America. Webster, who computed the response of a flow field to stationary forcing, using two-layer baroclinic models, demonstrated that equatorial heating and cooling does indeed produce a flow field which resembles Matsuno's solution. Furthermore, he suggested that the westerly jet predominating in the upper troposphere of the eastern Pacific may be regarded as a so-called "Walker circulation." The distribution of the annual mean vertical motion in the model tropics indicates that general upward motion exists in the tropical part of the western Pacific and general downward motion occurs in the eastern Pacific. Furthermore, in the lower troposphere (i.e., the 835-mb level) of the eastern Pacific, one can find an easterly jet along the equator. These features are in excellent agreement with the features of the Walker circulation as described, for example, by Bjerknes (1969). A similar circulation also exists over the Atlantic Ocean of the model.

The streamline-map of the 190-mb level also indicates that the mid-point of the line segment connecting the centers of the pair of anticyclones in the western Pacific is located slightly to the north of the equator. Furthermore, cross-equatorial flow of significant intensity can be seen in the central Pacific and in the Atlantic. The deviation of flow pattern from symmetry relative to the equator may result from nonsymmetry in the heating function. By using his model computation, Webster demonstrated that non-symmetric heating can be responsible for a flow field which is not symmetric relative to the equator.

Examining the maps of streamlines at all finite-difference levels, some of which are shown in Fig. 5.4, one finds that the northern anticyclone of the western Pacific pair discussed above is connected with the anticyclone over the Aleutian Archipelago, which appears in the streamline map for the 65-mb level. In other words, the axis of this anticyclone tilts toward the northeast with increasing height. It is surprising to the authors that the disturbance spans such a wide range of latitude.

The seasonal variation of streamlines in the upper troposphere are shown in Fig. 5.5, which contains maps of one-month mean streamlines at the 190-mb level for four months of the model year. Throughout the year, one can identify the pair of anticyclones discussed above the western Pacific of the model. However, the intensity of these anticyclones varies with respect to season. Sometimes other pairs of anticyclones are also identifiable over Africa and Central America where centers of intense precipitation are located.

One of the notable features of the upper tropospheric flow is the cross-equatorial flow associated with these anticyclone pairs. In January, southeasterly wind of significant intensity crosses the equator over Africa, the western Pacific, and South America and is responsible for the net northward transport of mass across the equator in the upper troposphere of the model (see Fig. 3.4). In July, the general direction of the cross-equatorial flow is reversed. A very intense northeasterly wind predominates in the Eastern Hemisphere and transports large quantities of mass from the Northern to the Southern Hemisphere. Johnson (1969) pointed out that these stationary flows transport angular momentum from the Northern to the Southern Hemisphere in January and in the opposite direction in July as a result of the correlation between the zonal and the meridional components of the wind. However, this transport is offset by the transport of angular momentum effected by the net mass flow in the opposite direction. This subject will be discussed again in the section dealing with the budget of angular momentum in the model tropics.

Fig. 5.5 indicates that the mid-oceanic troughs discussed earlier predominate during the summer season. In the Northern Hemisphere, these troughs predominate over the eastern Pacific and the mid Atlantic in July; whereas in the Southern Hemisphere, oceanic troughs intensify in January. As pointed out in the discussion on the annual mean flow, the mid-oceanic troughs in the Southern Hemisphere extend to the Northern Hemisphere and are responsible for cross-equatorial flow over the central Pacific.

The streamlines in the upper troposphere of the model, which have been discussed in the preceding paragraph, may be compared with the corresponding flow field in the actual atmosphere shown in Fig. 5.6. According to this comparison, various features of the flow field in the upper troposphere of the model are in excellent qualitative agreement with those of the actual atmosphere. In January, three pairs of anticyclones around the equator and an intense trough in the South Pacific are evident in both observed and computed flow fields. In July, a so-called easterly jet

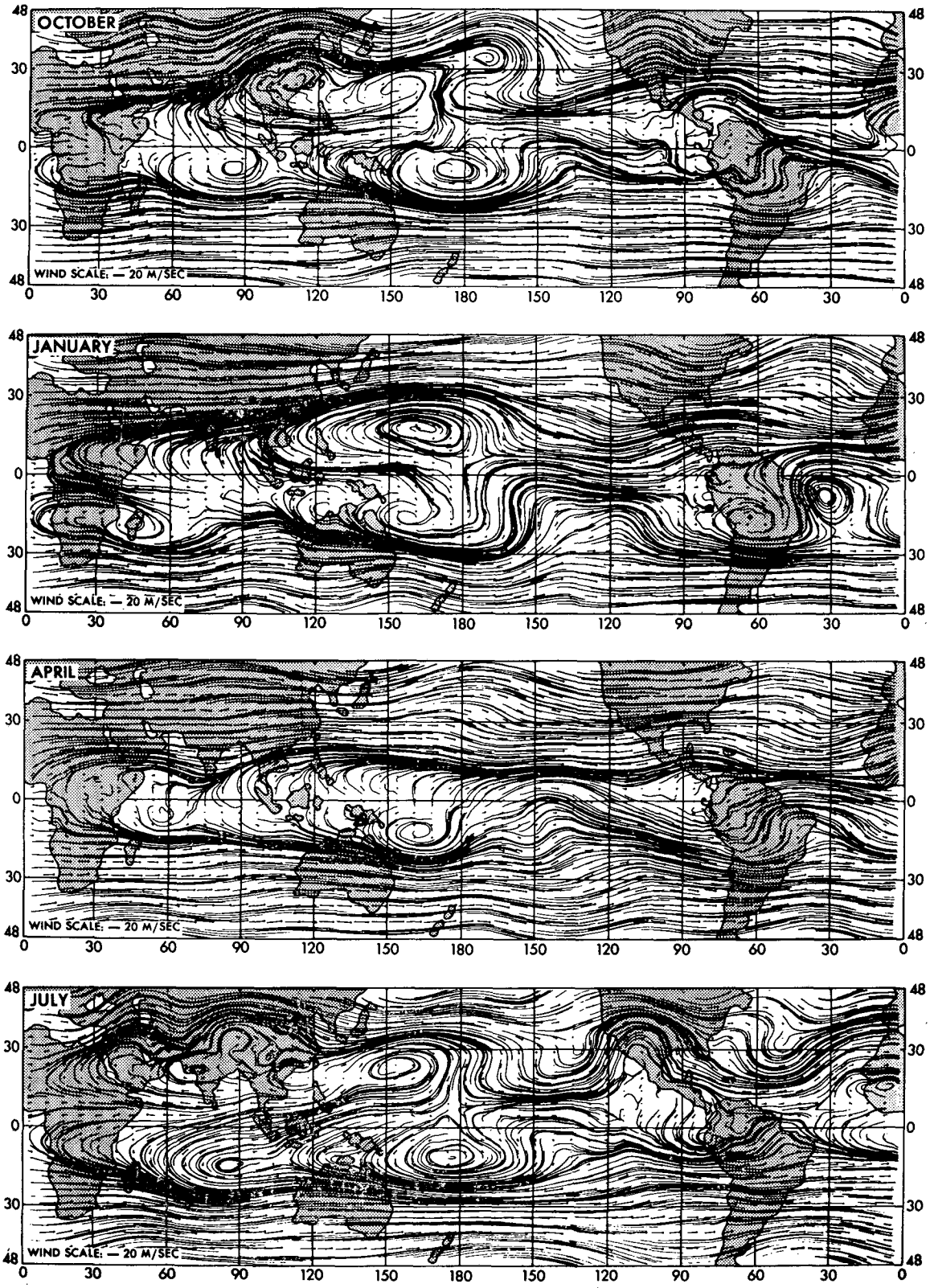

FIG. 5.5. One-month mean vectors and streamlines at the 190-mb level of the model during October, January, April and July. The length of the wind vectors is proportional to the wind speed. The length of a 20 m sec^{-1} vector is shown in the lower left-hand corner of each map.

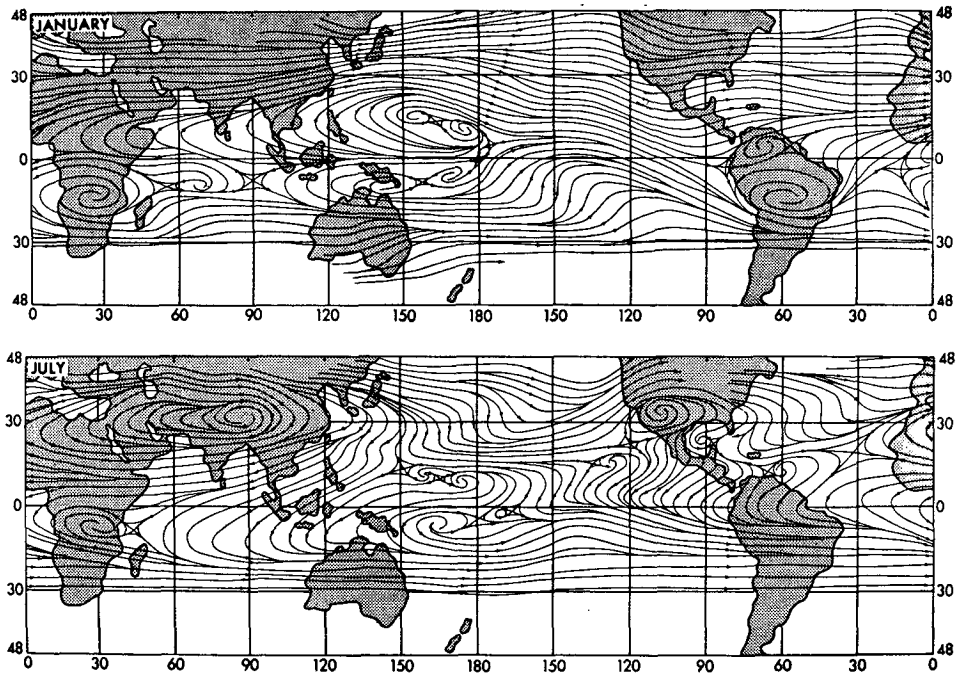

FIG. 5.6. Observed 1-month mean streamlines at the 200-mb level during January and July (Sadler, 1972)

extending from the western Pacific to the mid-Atlantic, and troughs over both the Pacific and the Atlantic of the Northern Hemisphere are simulated by the model.

Further examination of the results, however, reveals significant discrepancies between the observed and the computed flow fields. For example, the easterly jet

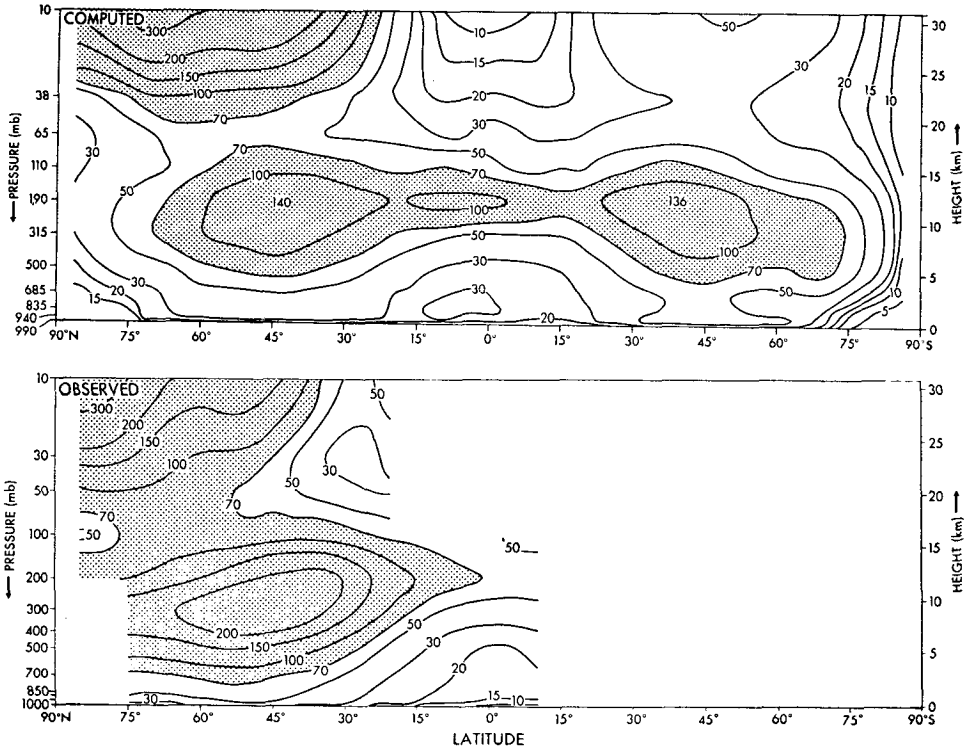

FIG. 6.1. Latitude-height distributions of the annual mean eddy kinetic energy (10^{-3} J cm^{-2} mb^{-1}): top, model distribution; bottom, observed distribution. [At and below the 100-mb level, the data compiled by Oort and Rasmusson (1971) are used. Above the 100-mb level, the results of Richards (1967) are adopted]. Values larger than 70 are shaded.

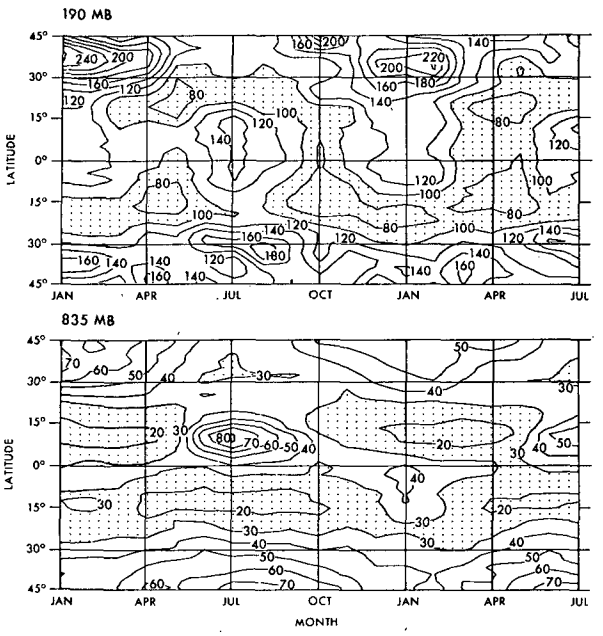

FIG. 6.2. Latitude-time distribution of eddy kinetic energy (10^{-3} J cm^{-2} mb^{-1}) in the model: top, 190-mb level; bottom, 835-mb level. Values smaller than 100 are shaded in the upper graph, and smaller than 30 in the lower.

mentioned above is located at too low a latitude by several degrees. In addition, the anticyclonic vortex extending zonally over the western Pacific, Africa and Asia in July is situated too far south by about 10°. It extends too far into the western Pacific reflecting the excessive development of tropical cyclones in the lower troposphere of the model (see subsection 5a). The causes of these discrepancies are yet to be identified.

6. Eddy kinetic energy

The annual mean distribution of eddy kinetic energy in the model tropics is shown in the upper half of Fig. 6.1 as a function of latitude and height. According to this figure, the eddy kinetic energy in the tropical part of the model atmosphere is greatest in the upper troposphere and decreases rapidly with height in the stratosphere. In the troposphere, it decreases generally with decreasing height except that a secondary maximum is evident in the tropics of the Northern Hemisphere of the model. It seems to be significant that eddy kinetic energy in the model tropics is not distributed symmetrically relative to the equator, i.e., it is larger in the Northern Hemisphere. Similar asymmetry exists in the distribution of sea surface temperatures, meridional circulation, and precipitation as already pointed out in preceding sections. The distribution of eddy kinetic energy in the model tropics described above may be compared with the distribution in the actual tropics shown in the bottom half of Fig. 6.1. This figure indicates that eddy kinetic energy in the actual tropics is at a maximum around the 200-mb level agreeing with the features of the model distribution. However, the magnitude of the maximum is significantly less than the eddy kinetic energy in the upper troposphere of the model. The causes for these discrepancies have not been identified.

The seasonal variation of eddy kinetic energy is illustrated in Fig. 6.2, which shows the latitude-time distributions of eddy kinetic energy at two isobaric levels of the model. According to this figure, the belt of maximum eddy kinetic energy in the lower troposphere of the model shifts from one hemisphere to another with respect to season. It moves from about 10N in July to about 4S in January. Comparing Fig. 6.2 and the latitude-time distribution of precipitation rate shown in Fig. 4.4, one finds that, in the model tropics, the seasonal movement of the maximum eddy kinetic energy in the lower troposphere resembles very well the movement of the rainbelt. However, the magnitude of eddy kinetic energy in the tropical rainbelt does not necessarily vary in proportion to the rate of precipitation there. For example, eddy kinetic energy is at a local maximum but is not particularly large in the lower troposphere over the model equator in March and April when the precipitation rate is very great. On the other hand, both eddy kinetic energy and precipitation rate are very large at about 10N in July. Further study is required to determine whether the preferred latitude for the development of tropical disturbances differs from that for the formation of the rainbelt in the model tropics.

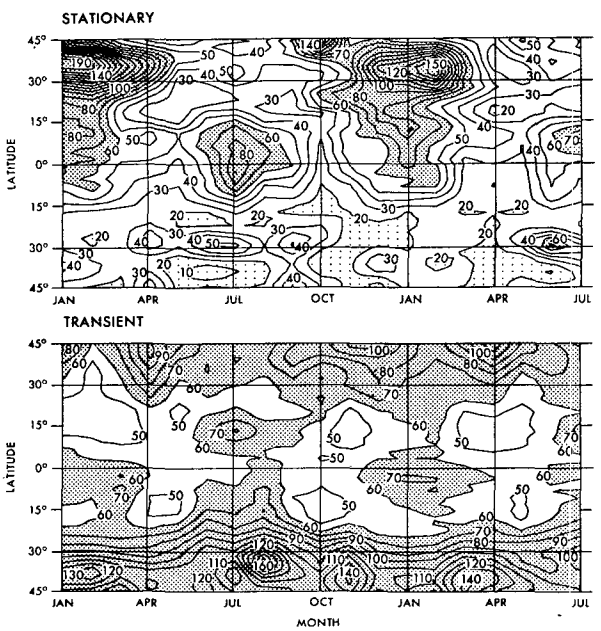

FIG. 6.3a. Latitude-time distribution of eddy kinetic energy (10^{-3} J cm^{-2} mb^{-1}) at the 190-mb level of the model: top, stationary component; bottom, transient component.

In the upper troposphere of the model tropics, eddy kinetic energy varies in a different manner. It has a semi-annual rather than an annual variation at the equator. The area of maximum eddy kinetic energy is centered about the equator and does not move from one hemisphere to another. In other words, the seasonal variation of eddy kinetic energy in the upper troposphere of the model tropics is more or less symmetric relative to the equator and does not follow the seasonal movement of the tropical rainbelt.

The eddy kinetic energy described above may be divided into two components—the kinetic energy of the stationary eddies and that of the transient eddies. Such a subdivision is useful for providing insight into how stationary are disturbances in the model tropics. In this study, the kinetic energy of stationary disturbances is defined by

$$K_E^{ST}=\tfrac{1}{2}\overline{[(\overline{u}^{t}-\overline{\overline{u}^{t}}^{\lambda})^2+(\overline{v}^{t}-\overline{\overline{v}^{t}}^{\lambda})^2]}^{\lambda}, \qquad (6.1)$$

and that of transient eddies is given by

$$K_E^{TR}=\tfrac{1}{2}\overline{\{\overline{[(u-\overline{u}^{\lambda})-(\overline{u}^{t}-\overline{\overline{u}^{t}}^{\lambda})]^2}^{t}}^{\lambda} +\overline{[(v-\overline{v}^{\lambda})-(\overline{v}^{t}-\overline{\overline{v}^{t}}^{\lambda})]^2}^{t}\}^{\lambda}, \qquad (6.2)$$

where u and v are eastward and northward components of the wind, respectively, and $\overline{(\ )}^{t}$ and $\overline{(\ )}^{\lambda}$ denote the time mean (over a period of one month) and the zonal mean, respectively. In rough terms, the stationary eddies defined here have a time scale longer than one month and include quasi-stationary disturbances such as the monsoon flow. The transient eddies defined here have a time scale shorter than one month and include tropical disturbances such as mixed Rossby gravity waves, equatorial Rossby waves and easterly waves, as well as ultra-long waves extending from middle latitudes (see Hayashi, 1973).

Fig. 6.3 shows how the kinetic energy of stationary and transient disturbances in the model tropics varies with respect to season. In the lower troposphere of the model, the zones of maximum eddy kinetic energy of both stationary and transient disturbances move from one hemisphere to another in a manner similar to that of the tropical rainbelt. In the upper troposphere of the model, the kinetic energy of stationary eddies varies by more than a factor of 2 from one season to another, reflecting the seasonal variation of monsoon activity. It is greatest around January and July when the cross-equatorial monsoon flow is at a maximum. On the other hand, the kinetic energy of transient eddies in the upper troposphere varies less with respect to season. One can nevertheless detect a seasonal shift of a maximum from one hemisphere to another which resembles the seasonal variation of eddy kinetic energy in the lower troposphere of the model tropics.

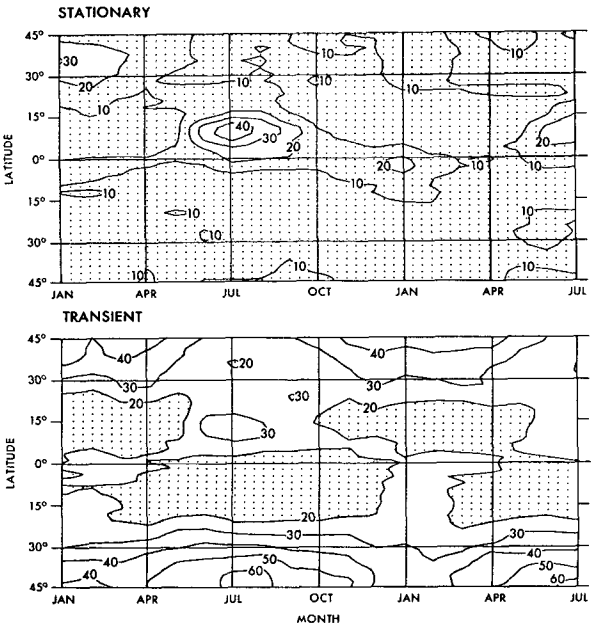

FIG. 6.3b. As in Fig. 6.3a except for the 835-mb level.

The geographical distribution of transient disturbances in the lower troposphere of the model tropics is illustrated in Fig. 6.4. The transient component of eddy kinetic energy presented in this figure is given by[4]

$$\overline{[(u-\overline{u}^{t})^2+(v-\overline{v}^{t})^2]}^{t}.$$

Comparing this figure with the distributions of the rate of precipitation shown in Fig. 4.2, one finds that the areas of relatively large transient eddy kinetic energy in the lower troposphere correspond very well with the location of the tropical rainbelt. In January, a belt of large transient eddy kinetic energy is located slightly to the north of the equator in the Pacific Ocean. It also branches from the central to the southeastern Pacific. The position of this belt agrees well with the location of the tropical rainbelt over the Pacific Ocean of the model. In the western part of the Indian Ocean, the area of large eddy kinetic energy is located around the island of Madagascar, where the rate of precipitation is very large in January. Similarly, in July one can find good correspondence between the areas of large transient eddy kinetic energy in the lower troposphere and the locations of the tropical rainbelt. For example, areas

[4] This expression is inconsistent with Eq. (6.2). However, the difference between the two transient kinetic energies is small.

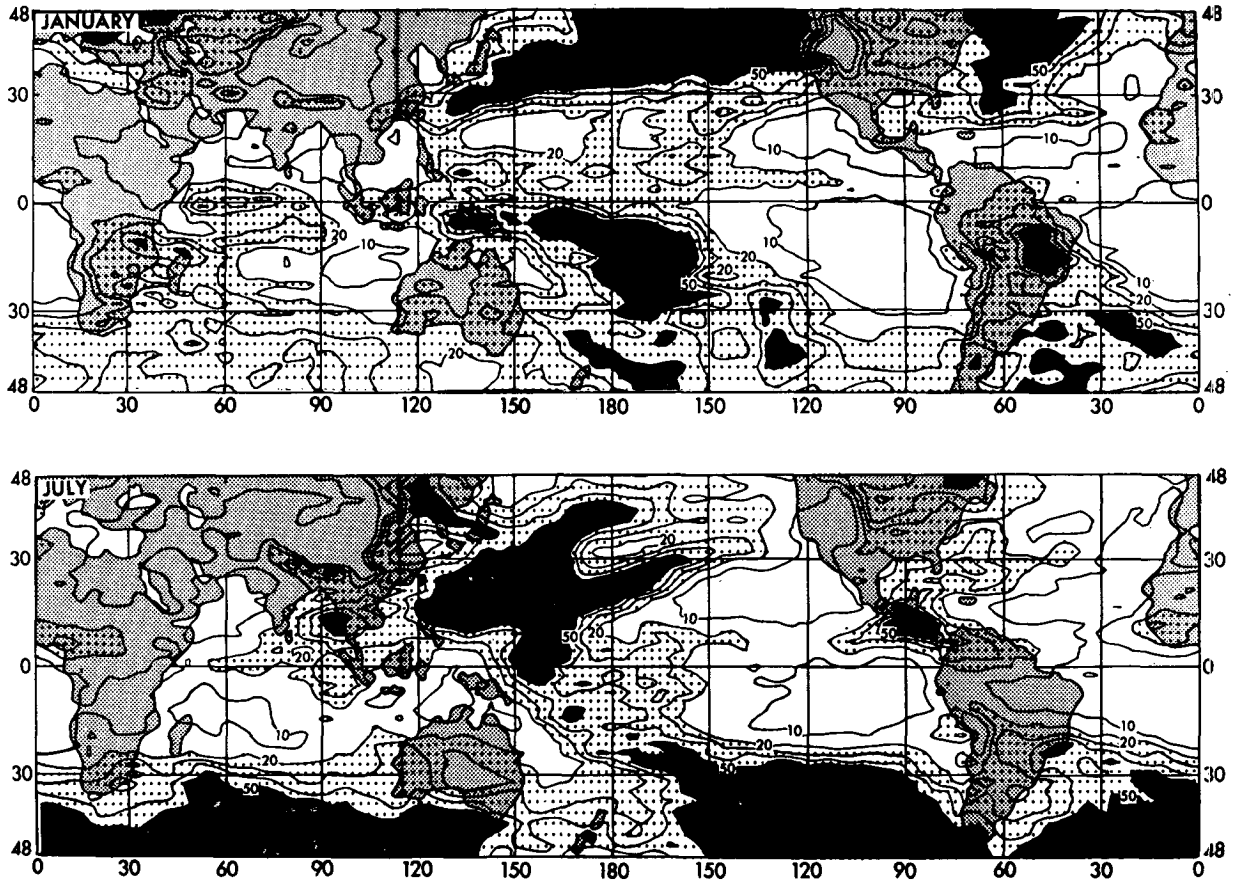

FIG. 6.4. Horizontal distribution of kinetic energy (m^2 sec^{-2}) of transient eddies at the 835-mb level of the model atmosphere: top, January; bottom, July. Black area, >50; large dots, 20–50; small dots, continental areas.

of large transient eddy kinetic energy in the western Pacific, the central Pacific and the Bay of Bengal correspond well with the areas of intense precipitation. It should be noted here that the regions of intense transient disturbances, which are identified above, approximately coincide with the areas of cyclogenesis in the actual tropics (see, e.g., Gray, 1968). As pointed out already, the rainbelt in the model tropics tends to form in areas of relatively warm sea surface temperatures. The results described here suggest that warm sea surface temperatures stimulate not only precipitation but also the development of transient disturbances in the model atmosphere. The mechanism of such stimulation will be discussed in the following section.

The horizontal distribution of eddy kinetic energy of transient eddies in the upper troposphere of the model tropics is shown in Fig. 6.5. According to this figure, the correspondence between the areas of large eddy kinetic energy and those of heavy precipitation is less obvious in the upper troposphere than it is in the lower troposphere. One can nevertheless identify some areas of large eddy kinetic energy corresponding to areas of maximum precipitation, i.e., the areas in the central and the western Pacific (in the Southern Hemisphere) in January and those in the western Pacific, Central America, and the Bay of Bengal (in the Northern Hemisphere) in July.

In summary, disturbances in the model tropics tend to develop in certain geographical regions, i.e., oceanic regions with relatively warm sea surface temperatures. This tendency is particularly evident in the lower troposphere.

7. Budget of eddy kinetic energy

a. Basic equations

In the preceding section, the distribution of eddy kinetic energy and its seasonal variation were described. The subject of this section is the budget of eddy kinetic energy in the model tropics. In preparation for the discussion of the energy budget, it is desirable to write down the basic equations.

The equation for zonal mean eddy kinetic energy on an isobaric surface is

$$\frac{\partial k_E}{\partial t}=[-\overline{D(k_E)}^{\lambda}+\langle k_Z\cdot k_E\rangle-\overline{\mathbf{V}'\cdot\nabla\phi'}^{\lambda}+\overline{\mathbf{V}'\cdot\mathbf{F}'}^{\lambda}], \quad (7.1)$$

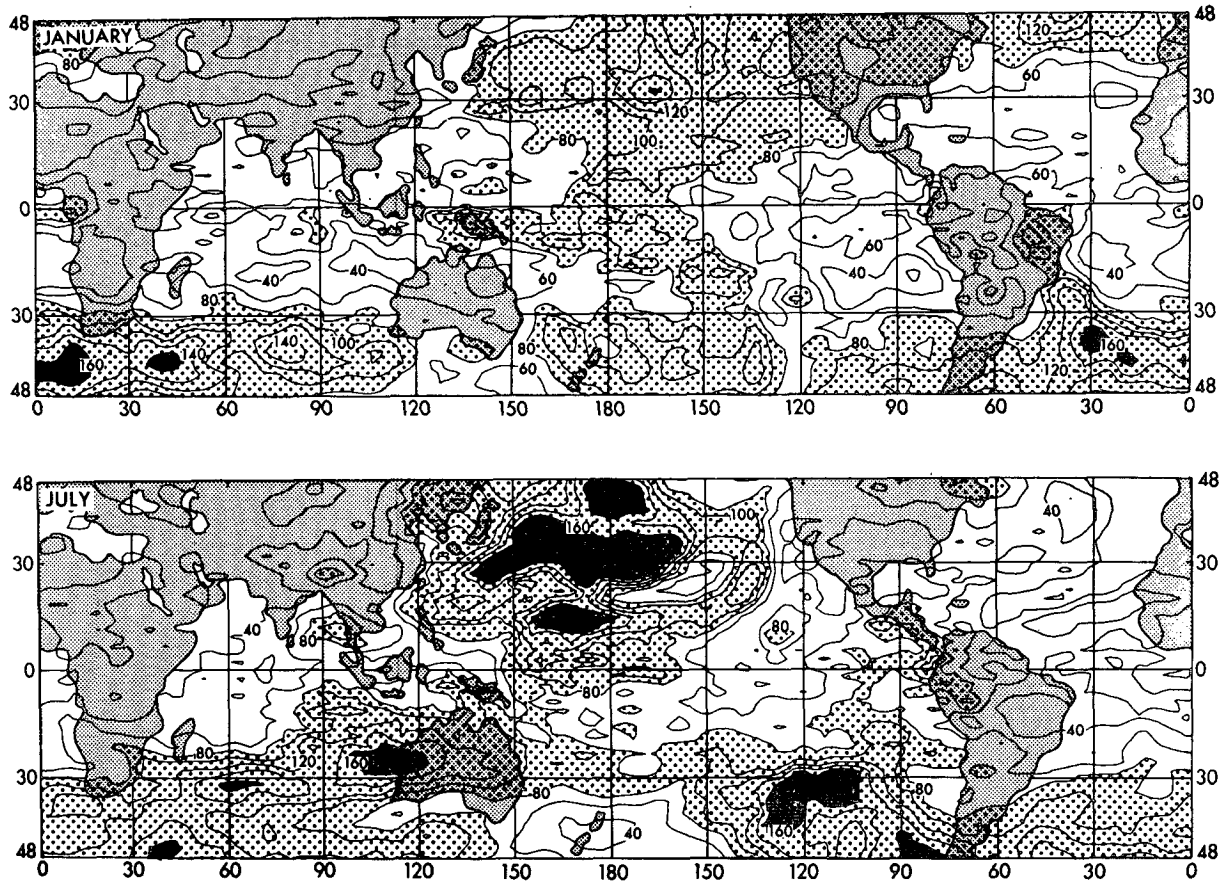

FIG. 6.5. As in Fig. 6.4 except for the 190-mb level. Black area, >160; large dots, 80–60; small dots, continental areas.

where

$$k_E = k_T - k_Z, \tag{7.2}$$

$$k_T = \tfrac{1}{2}(u^2+v^2), \tag{7.3}$$

$$k_Z = \tfrac{1}{2}[(\overline{u}^{\lambda})^2+(\overline{v}^{\lambda})^2], \tag{7.4}$$

$$\overline{D(\ )}^{\lambda} = \frac{1}{a\cdot\cos\theta}\frac{\partial}{\partial\theta}[\cos\theta\cdot\overline{v\cdot(\ )}^{\lambda}]+\frac{\partial}{\partial p}[\overline{\omega(\ )}^{\lambda}], \tag{7.5}$$

$$\langle k_Z\cdot k_E\rangle = \left(\frac{\overline{u}^{\lambda}}{\cos\theta}\right)\overline{D(u'\cdot\cos\theta)}^{\lambda} + \overline{v}^{\lambda}\left[\overline{D(v')}^{\lambda}+\frac{\tan\theta}{a}\overline{(u'^2)}^{\lambda}\right], \tag{7.6}$$

t is time, a the radius of the earth, $\mathbf{V}$ the horizontal wind vector, u and v the east and northward components of the wind, ω the vertical p-velocity, θ latitude, p pressure, ϕ geopotential height, and $\mathbf{F}$ the frictional force vector. The symbols $\overline{(\ )}^{\lambda}$ and $(\ )'$ indicate zonal mean and its deviation. In the following discussion, the

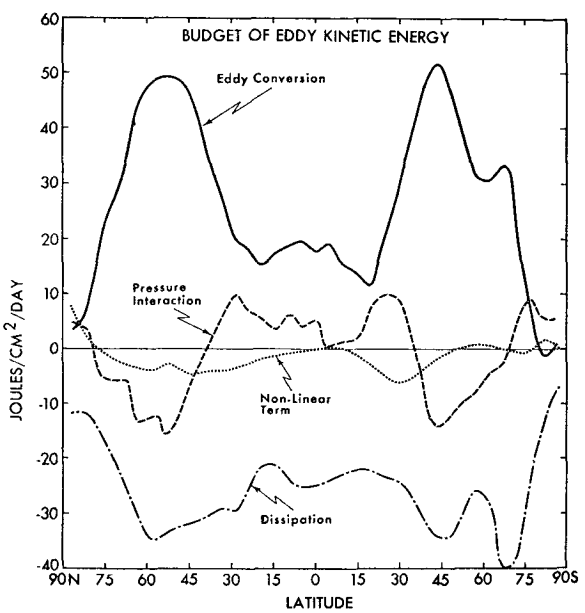

FIG. 7.1. Annual mean latitudinal distribution of the vertical mass-weighted integral of various components of the budget of eddy kinetic energy: solid line, eddy conversion; dashed line, pressure integration; dotted line, nonlinear term; dot-dashed line, dissipation.

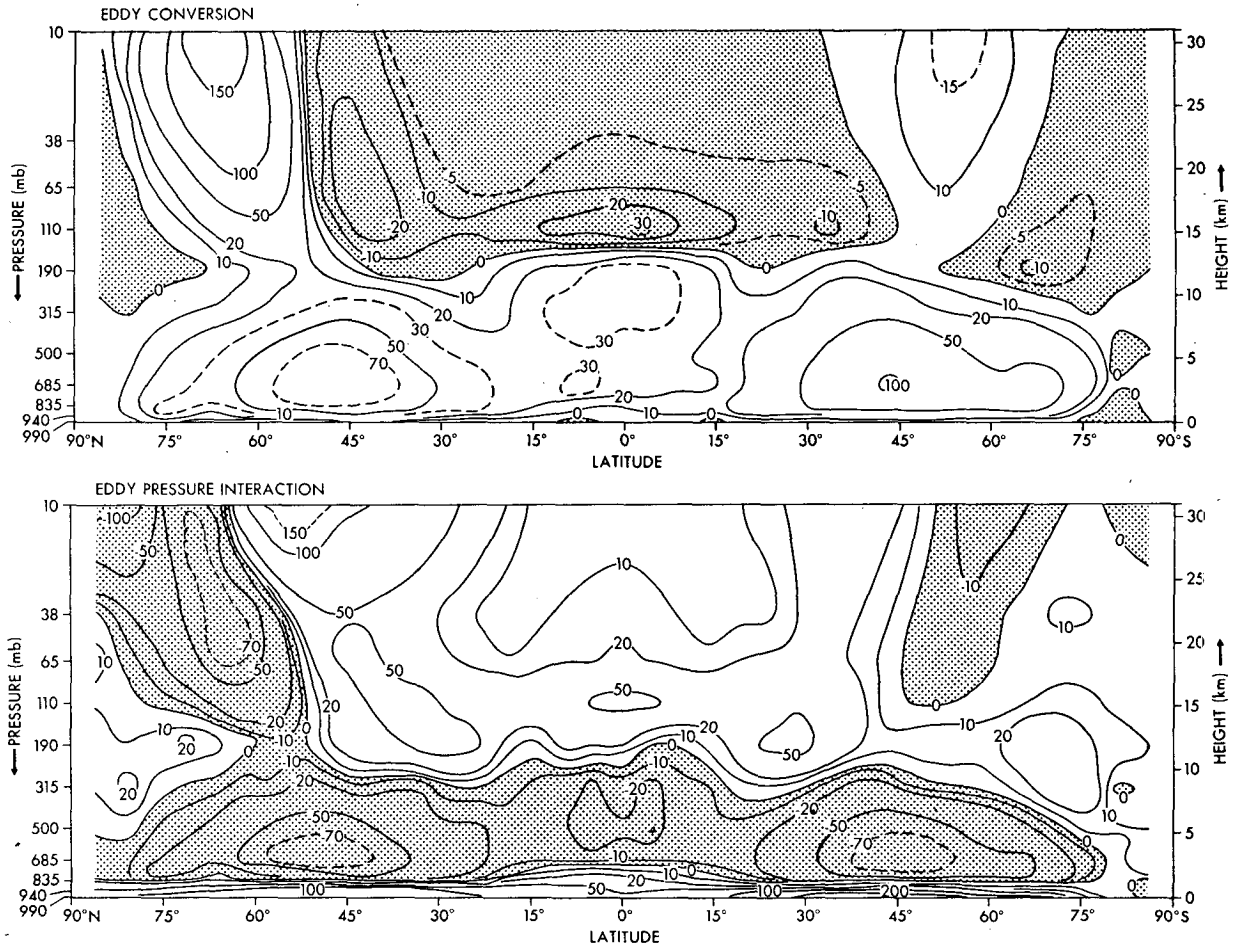

FIG. 7.2. Latitude-height distribution of annual mean rate of eddy conversion (top) and of the annual mean rate of the convergence of energy flux through eddy pressure interaction (bottom). Units are 10^{-3} J cm^{-2} mb^{-1} day^{-1}. Negative areas are shaded.

sum of the first two terms in the square brackets of (7.1) will be called the nonlinear term, the third term $\overline{(-\mathbf{V}'\cdot\nabla\phi')}^{\lambda}$ the production term (of the eddy kinetic energy), and the fourth term $\overline{(\mathbf{V}'\cdot\mathbf{F}')}^{\lambda}$ the eddy dissipation term. The nonlinear term can be separated into two terms: the first represents the flux convergence of eddy energy $-\overline{D(k_E)}^{\lambda}$, and the second represents energy transfer from zonal to eddy kinetic energy $\langle k_Z\cdot k_E\rangle$. The production term may also be divided into two parts:

$$-\overline{\mathbf{V}'\cdot\nabla\phi'}^{\lambda}=-\overline{\omega'\alpha'}^{\lambda}-\overline{D(\phi')}^{\lambda}, \qquad (7.7)$$

where α is specific volume, the first term represents the conversion of eddy available potential energy to eddy kinetic energy (the eddy conversion term), and the second term represents the energy exchanged by the eddy-component of pressure interaction (the eddy pressure interaction term).

b. Annual mean

The annual mean distribution of the vertical mass-weighted integrals of various components of the budget of eddy kinetic energy are shown as a function of latitude in Fig. 7.1, which clearly shows that the most important source of eddy kinetic energy in the model tropics is the conversion of eddy potential energy into eddy kinetic energy. A secondary source is the energy supplied to the tropics from middle latitudes through eddy pressure interaction. The net effect of the nonlinear term is small and negative. It is noteworthy that the contribution of eddy pressure interaction is largest in the subtropics where the rate of eddy conversion is relatively small. Fig. 7.1 also shows that the distributions of these two effects tend to be correlated negatively with each other in low as well as in high latitudes. In other words, eddy pressure interaction transports energy from the areas of high rates of eddy conversion to areas of low eddy conversion. This tendency becomes more evident when one examines the seasonal variation of the energy budget described in

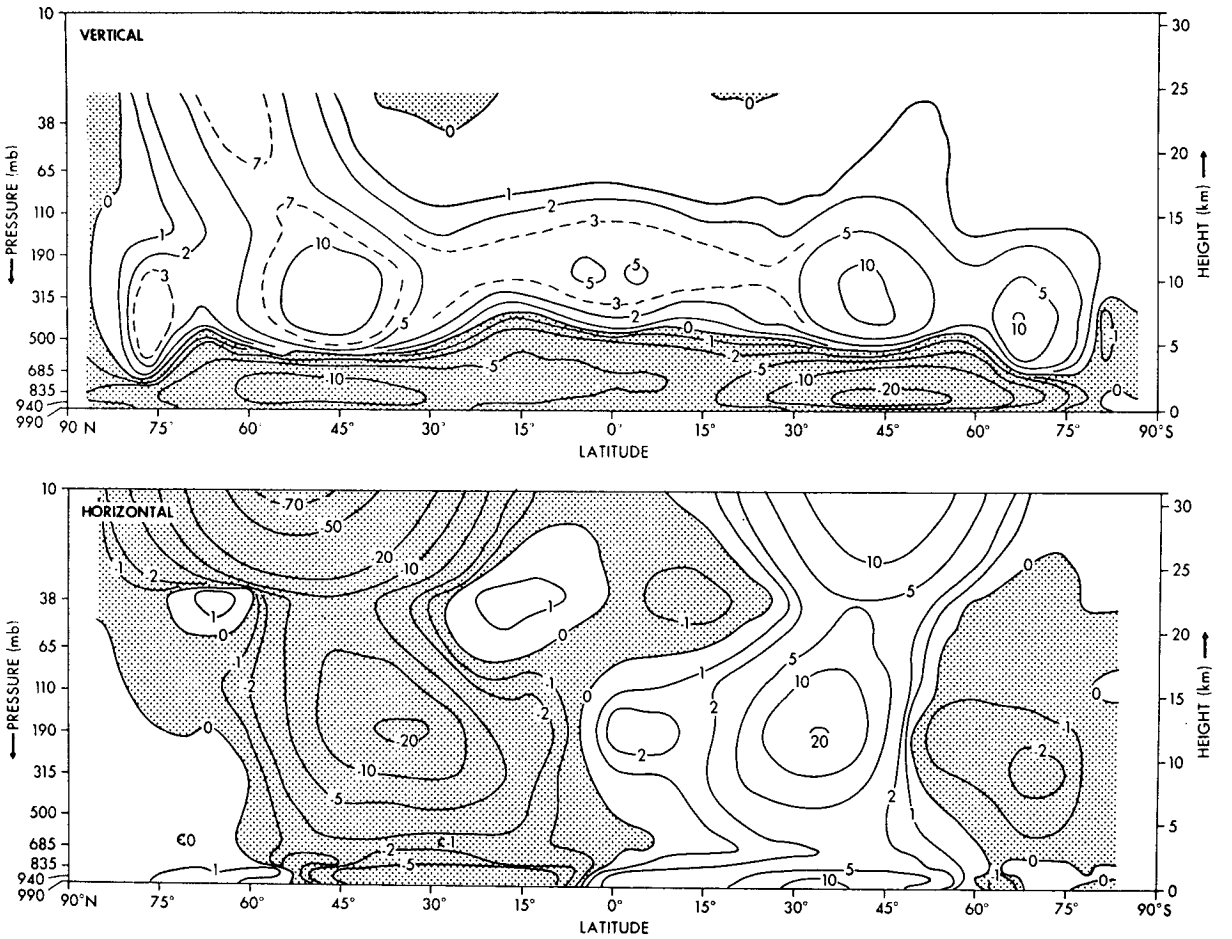

FIG. 7.3 Annual mean latitude-height distributions of energy flux due to eddy pressure interaction: top, upward flux (J cm^{-2} day^{-1}); bottom, northward flux (10^{15} J mb^{-1} day^{-1}). Negative (downward and southward) areas are shaded.

the latter part of this section. The importance of eddy conversion in maintaining the tropical disturbances is emphasized by Manabe and Smagorinsky (1967), Manabe *et al.* (1970) and Nitta (1970). The positive contribution of the effect of eddy pressure interaction in maintaining the kinetic energy of the tropical disturbances is discussed by Mak (1969) in a theoretical study.

To examine how eddy kinetic energy is maintained at various altitudes in the model tropics, latitude-height distributions of eddy conversion and eddy pressure interaction are given in Fig. 7.2. In addition, latitude-height distributions of the upward and northward components of energy flux through pressure interaction are shown in Fig. 7.3. In the tropics, eddy conversion is at a maximum in the 200–500 mb layer from where energy is exported both upward and downward through eddy pressure interaction. The downward flux is responsible for supplying energy to the planetary boundary layer where dissipation of eddy kinetic energy is very intense. The upward flux converges mainly around the equatorial tropopause and in the lower stratosphere and is responsible for maintaining eddy kinetic energy there. The horizontal flux of energy through pressure interaction is at a maximum in the upper troposphere and transfers energy from middle latitudes toward lower latitudes. It converges mainly in the subtropics, as previously discussed. The effects of positive eddy conversion together with the smaller positive contribution of pressure interaction are responsible for the maximum eddy kinetic energy around the 200-mb level of the model equator. These features of the energetics in the model tropics are in qualitative agreement with those of the actual tropics, as investigated by Nitta (1970).

c. Seasonal variation

The seasonal variations of eddy conversion and eddy pressure interaction in the model atmosphere are given in Fig. 7.4; it shows that the zonal mean rate of eddy conversion is very large around 15N in July. In January, it is maximum slightly to the south of the equator. In general, the zone of maximum eddy conversion shifts

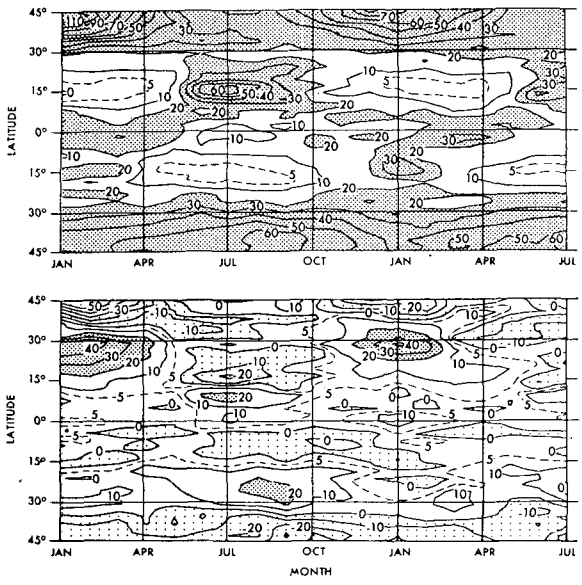

FIG. 7.4. Latitude-time distributions of vertical mass-weighted integrals: top, eddy conversion; bottom, eddy pressure interaction. Units are in J cm^{-2} day^{-1}. Values above 20 are darkly shaded. Negative values are lightly shaded.

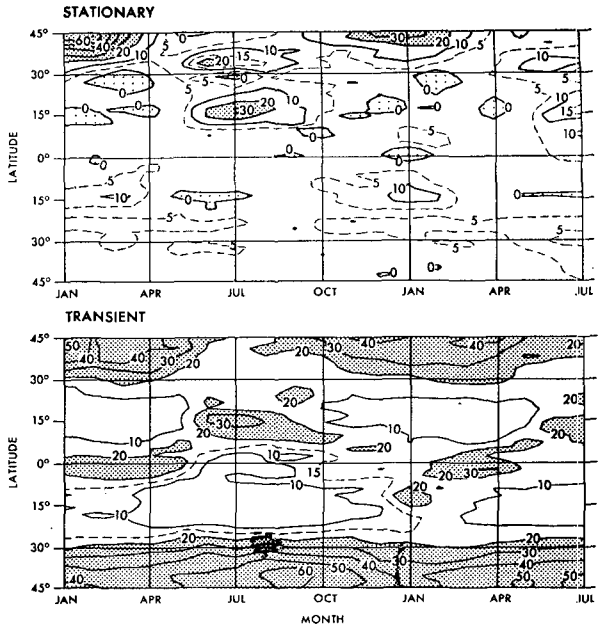

FIG. 7.6. Latitude-time distributions of vertical mass integrals of eddy conversion (J cm^{-2} day^{-1}): top, stationary component; bottom, transient component. Values above 20 are shaded.

from one hemisphere to the other in a manner similar to the movement of the rainbelt in the model tropics (see Fig. 4.4). On the other hand, the contribution of eddy pressure interaction tends to be at a maximum and is very important in the subtropics of the winter hemisphere where eddy conversion is small. It is minimum (slightly negative) in the tropics of the summer hemisphere where the rate of eddy conversion is maximum. In short, the effects of eddy conversion and that of pressure interaction tend to supplement each other in producing eddy kinetic energy in low latitudes. It should be emphasized here that the contribution of eddy pressure interaction is of major importance in the subtropics of the winter hemisphere although its annual mean value is relatively small. (Note that the seasonal variation of this effect is very large.)

The latitude-time distribution of the horizontal component of the energy flux due to eddy pressure interaction in the model atmosphere, given in Fig. 7.5, shows that the energy flux from middle latitudes converges the most in the subtropics of the winter hemisphere and contributes to the production of eddy kinetic energy there. This figure also indicates that in July eddy pressure interaction is responsible for transporting energy from the region of large eddy conversion around 15N toward the equator. In general, it tends to spread the eddy kinetic energy created by the conversion of eddy available potential energy over a wider area. In Section 6, it is shown that in the lower troposphere of the model tropics, the latitude of maximum eddy kinetic energy moves from one hemisphere to another in a manner similar to the seasonal variation of eddy conversion. On the other hand, the eddy kinetic energy in the upper troposphere does not necessarily undergo a similar variation. The results of the analysis described here indicate that this difference is caused by the effect of pressure interaction which predominates in the upper troposphere of the model atmosphere.

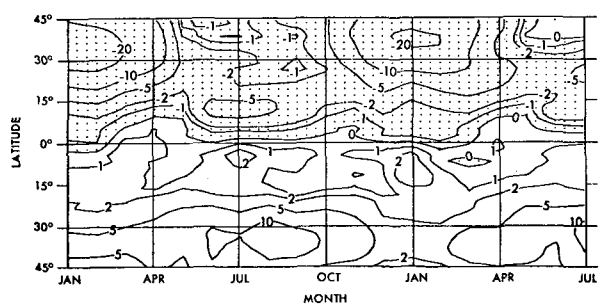

FIG. 7.5. Latitude-time distribution of the vertical mass-weighted integral of the northward energy flux due to eddy pressure interaction (sum of stationary and transient components) in the model atmosphere. Units are in 10^{18} J day^{-1}.

Eddy conversion may be subdivided further into stationary and transient components in the following manner:

(Stationary conversion)

$$= \int_0^{p*} \overline{(\omega - \bar{\omega}^t)(\alpha - \bar{\alpha}^t)}^{\lambda} \, dp \quad (7.8)$$

(Transient conversion)

$$= \int_0^{p*} [(\omega - \bar{\omega}^{\lambda}) - (\bar{\omega}^{t} - \bar{\omega}^{\lambda})][(\alpha - \bar{\alpha}^{\lambda}) - (\bar{\alpha}^{t} - \bar{\alpha}^{\lambda})]dp, \tag{7.9}$$

where P_* is surface pressure.

In Fig. 7.6, these two components of eddy conversion are shown as a function of latitude and time. This figure indicates that the belt of maximum transient eddy conversion shifts from one hemisphere to the other with the passage of seasons in a manner similar to the movement of the rainbelt in the model tropics. On the other hand, the stationary eddy conversion does not exhibit a similar variation with time. However, it is large during the summer season in each hemisphere.

The pressure interaction term may also be similarly subdivided into stationary and transient components. Figs. 7.7 and 7.8 show the seasonal variation of the northward flux of energy due to pressure interaction and that of the flux convergence, respectively. According to these figures, the stationary component of the eddy pressure interaction is mainly responsible for the energy flux from mid-latitudes to the subtropics of the Northern Hemisphere, whereas the transient component accounts for most of the energy flux into the subtropics of the Southern Hemisphere. Manabe and Terpstra (1974) attempted to identify the effects of mountains based upon results from a set of numerical

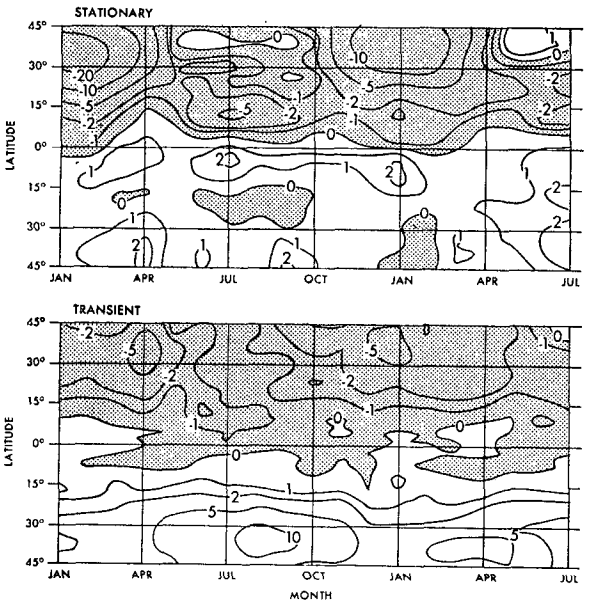

FIG. 7.7. Latitude-time distributions of the vertical mass-weighted integrals of northward energy flux due to pressure interaction (10^{18} J day^{-1}): top, stationary component; bottom, transient component. Negative (southward) areas are shaded.

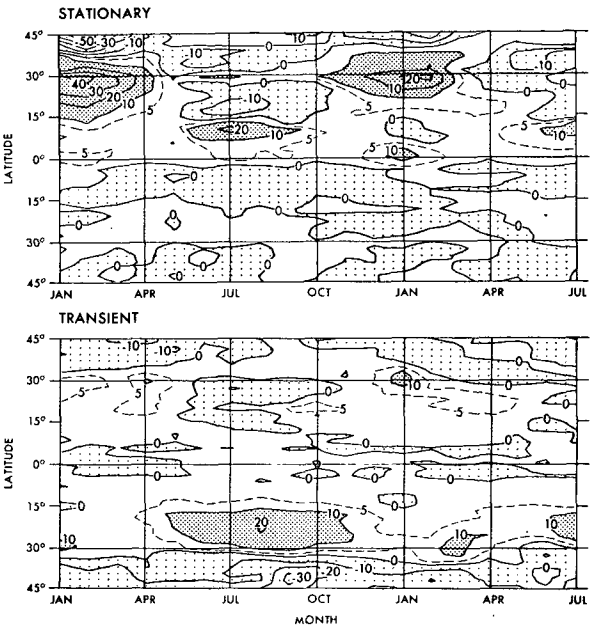

FIG. 7.8. Latitude-time distributions of the vertical mass-weighted integral of the rate of convergence of energy flux through eddy pressure interaction (J cm^{-2} day^{-1}): top, stationary component; bottom, transient component. Values above 10 are darkly shaded. Negative values are lightly shaded.

experiments. They suggest that major mountain ranges enhance the stationary component of eddy conversion in the Northern Hemisphere and are responsible for the large southward flux of energy through stationary eddy pressure interaction. In the Southern Hemisphere of their model, transient components of both eddy conversion and eddy pressure interaction prevail because of the lack of large-scale mountain ranges in middle latitudes. Therefore, it is probable that the difference in topography between the two hemispheres is responsible for the difference in the distributions of stationary and transient eddy pressure interaction fluxes mentioned above.

In Section 6 it is shown that warm sea surface temperatures tend to stimulate the development of the tropical rainbelt and the accompanying disturbances in the model tropics. We shall examine the geographical distribution of the rate of conversion of eddy available potential energy and discuss how the kinetic energy of such disturbances is maintained.

Figs. 7.9 and 7.10 show horizontal distributions of the transient and the stationary components of eddy conversion for January and July. The transient component of eddy conversion is defined by[5]

$$\int_0^{p*} \overline{(\omega - \bar{\omega}^{t})(\alpha - \bar{\alpha}^{t})}^{t} dp, \tag{7.10}$$

[5] This expression is inconsistent with Eq. (7.7). However, the difference between the two transient conversions is small.

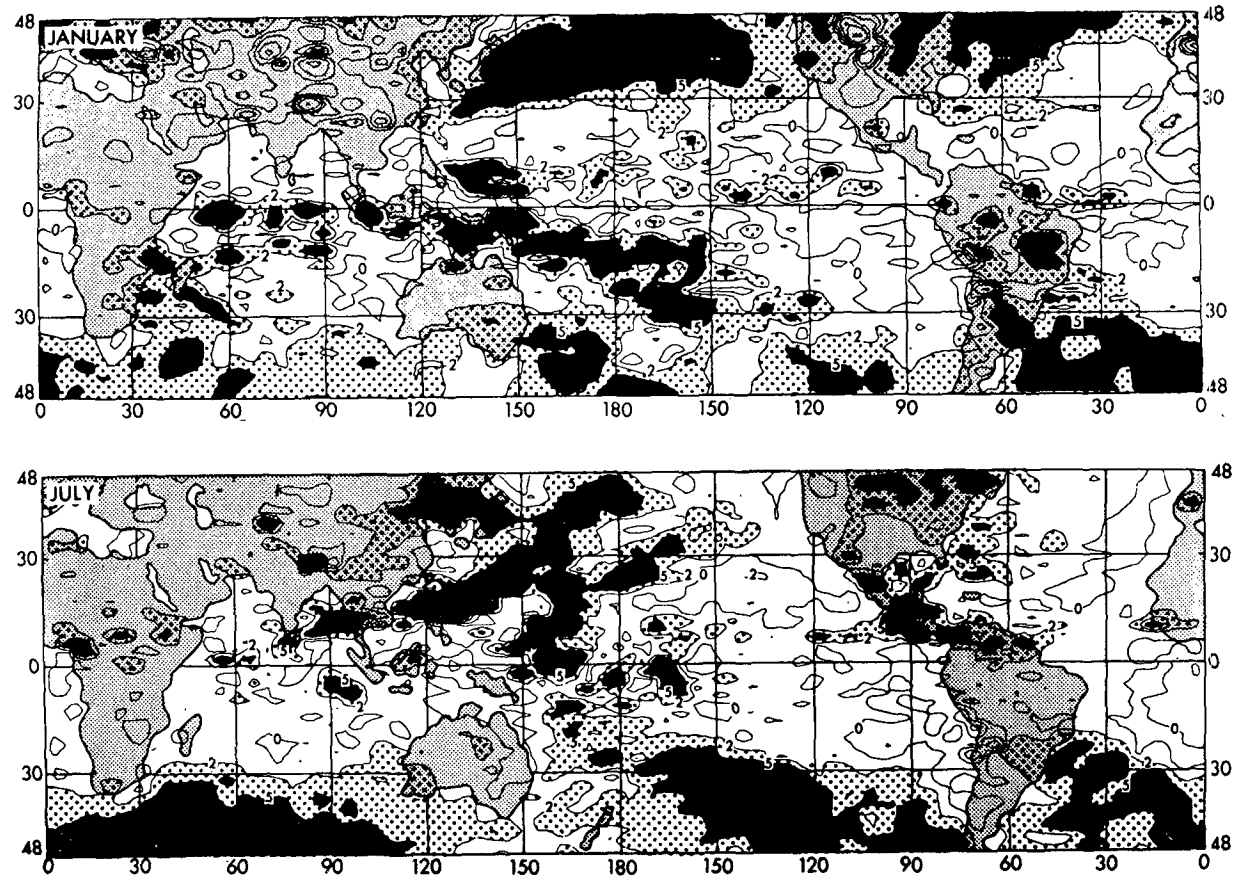

FIG. 7.9. Horizontal distribution of the vertical mass-weighted integral of the transient component of eddy conversion (ergs gm^{-1} sec^{-1}) for January (top) and July (bottom): black area, >5; large dots, 2 to 5; small dots, continental areas.

and the stationary component of eddy conversion by

$$\int_0^{p*} (\omega - \overline{\omega}^t)(\alpha - \overline{\alpha}^t)\,dp, \qquad (7.11)$$

where ω is the vertical p-velocity, α is specific volume, $\overline{(\,)}^t$ denotes a one-month mean, and $\overline{(\,)}^\lambda$ a zonal mean. According to these figures, both transient and stationary components of eddy conversion predominate in the general areas of relatively warm sea surface temperatures.

The reason why the conversion of eddy available potential energy is encouraged in the areas of relatively warm sea surface temperature is not obvious. However, it is probable that general upward motion develops in the area of warm sea surface temperatures and creates a humid air mass which encourages moist convective activities. As previously pointed out, one of the important characteristics of the general circulation model used for this study is the parameterization of the macroscopic effects of moist convection by "convective adjustment." Manabe and Smagorinsky (1967) and Manabe *et al.* (1970) show how the synoptic-scale disturbances develop in the tropics of this type of model. They point out that the disturbances have a warm core in the upper troposphere and a cold core in the lower troposphere resulting from execution of the moist convective adjustment. The intense upward motion in the warm core of the upper troposphere is responsible for the release of eddy available potential energy generated by moist convective processes. It was shown that warm sea surface temperatures tend to accelerate the development of tropical disturbances by destroying the cold core in the lower troposphere and raising the temperature of the warm core in the upper troposphere. These results account for the predominance of eddy conversion in areas of warm sea surface temperatures. Since quasi-stationary upward motion and moist convection prevail in areas of large stationary eddy conversion, they should encourage the transient component of eddy conversion as well. This partly explains the fact that the areas of large stationary eddy conversion tend to coincide with those of large transient eddy conversion. In summary, the results from both the present integration and past studies using similar

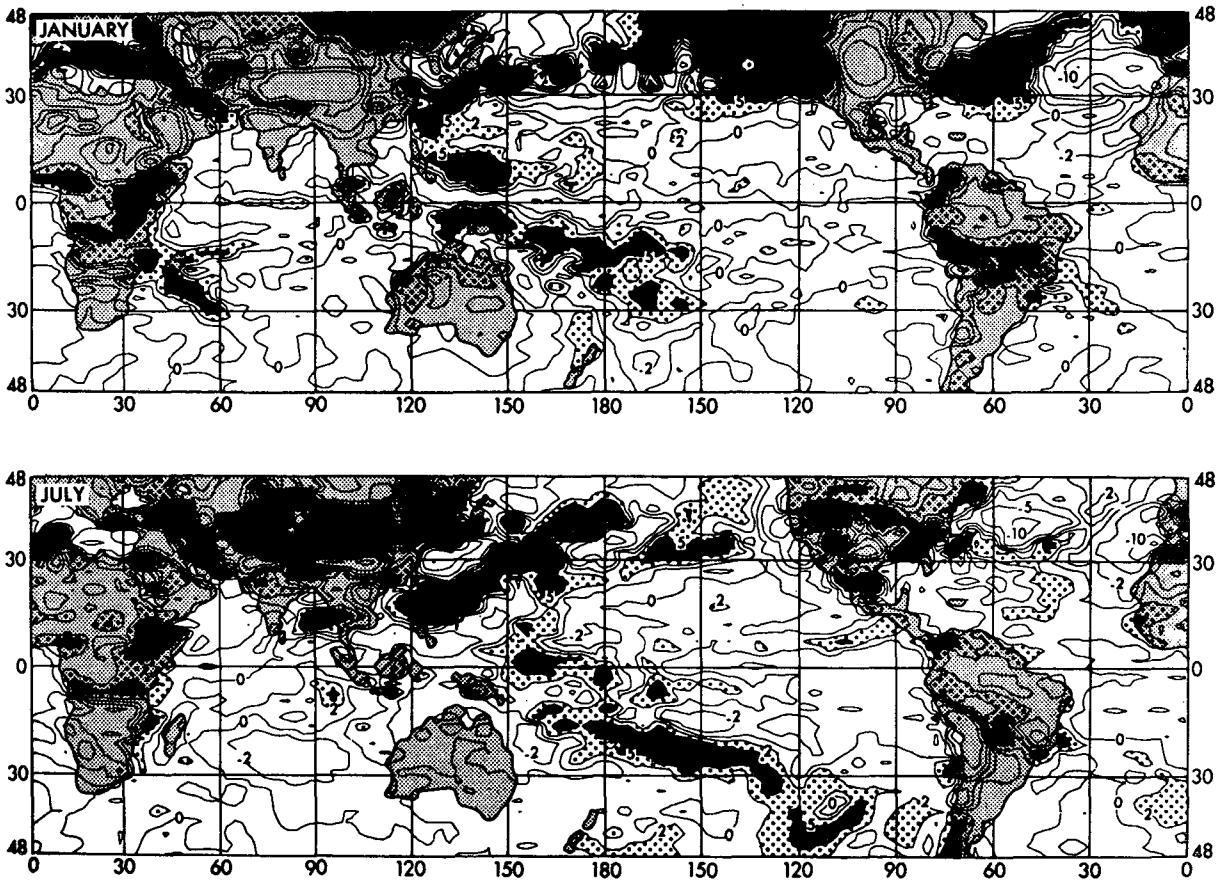

Fig. 7.10. As in Fig. 7.9 except for stationary component of eddy conversion.

models indicate that the enhancement of the conversion of potential energy by warm sea surface temperatures is very important factor in the development of the tropical rainbelt and the accompanying disturbances in the model tropics.

8. Heat, water and momentum budgets

a. Heat balance (annual mean)

The components of the heat balance in the model atmosphere are heating or cooling due to radiative transfer, the effect of meridional circulation, large-scale eddy processes, and convection and condensation. The contribution of horizontal mixing by subgrid-scale eddies is small. In this study, radiative transfer includes the effects of both solar and terrestrial radiation. Convection and condensation represent the net effects of moist convection and condensation as well as dry convection and vertical mixing by subgrid-scale eddies. In Fig. 8.1, the vertical distribution of these heat balance components at the equator of the model are compared with those of the subtropics. According to this figure, the meridional circulation exerts a cooling effect in the model tropics, but has a heating effect in the model subtropics. This difference is caused by the reversal of the sign of the vertical motion between the upward and downward branches of the Hadley cell, and is mainly counter-balanced by the difference in the intensity of the moist convective heating between the two regions. In the model tropics, the layer of intense moist convective heating extends to the upper troposphere, whereas in the model subtropics, the heating decreases rapidly with increasing height. (It is very large in the planetary boundary layer.) This is because the moist convection in the model subtropics is relatively shallow and does not penetrate as deeply as the convection in the model tropics.

The latitude-height distribution of the heating rate due to convection and condensation is shown in Fig. 8.2. Again, this figure illustrates the maximum in convective heating in the moist tropics and the minimum in heating in the dry subtropics. The general features of this distribution agree with those of the actual atmosphere estimated by Newell *et al.* (1972). However, the level of maximum heating in the model tropics (685-mb level) is located somewhat lower than that in the actual tropics (500-mb level) as obtained by Newell *et al.* (1972) and Nitta (1972).

It should be noted that large-scale eddies tend to

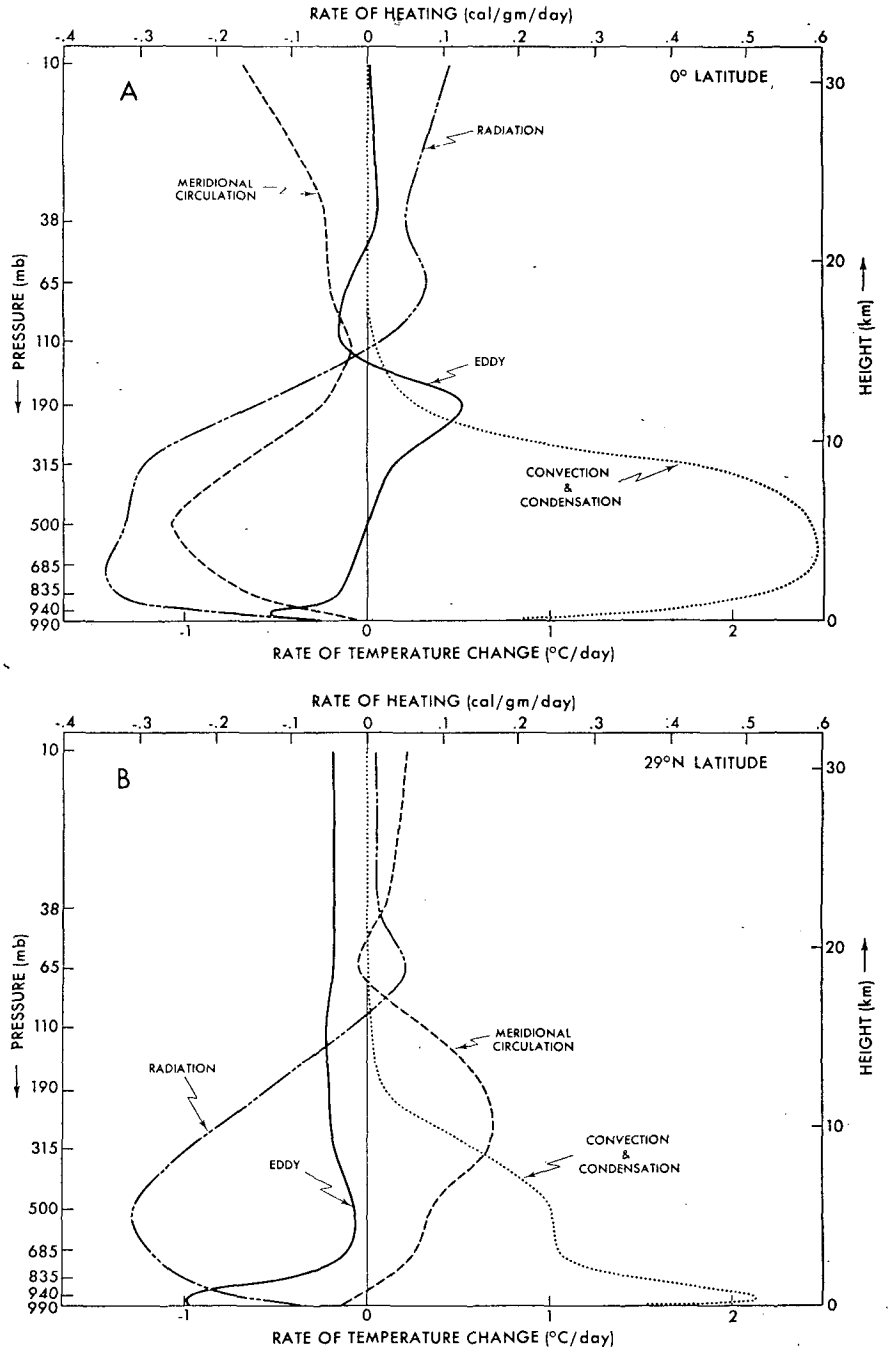

FIG. 8.1. Vertical distributions of annual mean heat balance components in the model atmosphere: top (A), zonal means at the equator; bottom (B), zonal means at 29N. Solid lines, the effect of large-scale eddies; dashed lines, the effect of meridional circulation; dotted lines, net contribution of condensation, moist and dry convection, and sensible heat flux from the earth's surface; dashed-dotted lines, net contribution of solar and longwave radiation.

increase the static stability of the model tropics by cooling the lower troposphere and heating the upper troposphere (see Fig. 8.1a). The results of our analysis indicate that large-scale eddies transport heat upward[6] in the model tropics and are partly responsible for this stabilizing effect. According to the results of Hayashi (1973), the mixed Rossby-gravity waves in the model tropics are responsible for the horizontal convergence of heat flux toward the equator[7] and also contri-

[6] One can infer this from the latitude-height distribution of the rate of conversion of eddy potential energy shown in Fig. 7.2.

[7] On the other hand, large-scale eddies are responsible for the horizontal divergence of heat flux in the lower stratosphere of the model.

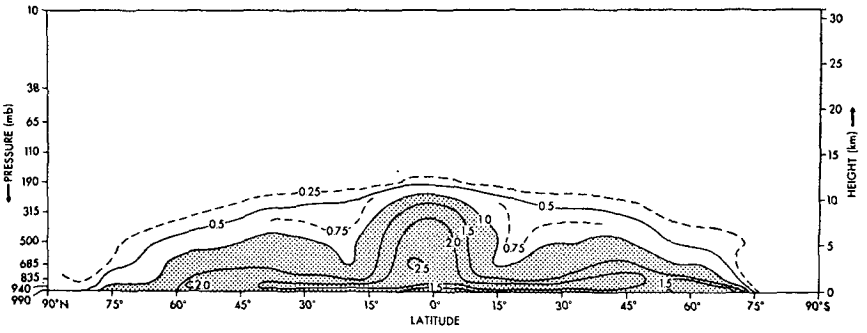

FIG. 8.2. Latitude-height cross section of the annual mean rate of temperature change due to moist and dry convection, condensation, and sensible heat flux from the earth's surface (°K day^{-1}). Values greater than 1.0 are shaded.

bute to the heating in the upper troposphere of the model.

b. Water balance (annual mean)

The factors which affect the budget of water vapor in the model tropics are 1) dry and moist convection (condensation) and evaporation, 2) meridional circulation, and 3) large-scale eddies. The contribution of horizontal mixing by subgrid-scale eddies is very small. Fig. 8.3a presents the vertical distributions of these components of the water balance at the equator of the model; it shows that the planetary boundary layer of the model tropics gains water vapor through the advection by meridional circulation and through evaporation and convection, whereas it loses water vapor through the transport by large-scale eddies. According to our analysis, the positive contribution of meridional circulation in Fig. 8.3a implies that the supply of water vapor by the equatorward branch of the Hadley cell exceeds the removal of moisture by the upward branch of the cell. Fig. 8.3a also suggests that, in the planetary boundary layer, the gain of water vapor due to the evaporation from the earth's surface overcomes the loss due to the condensation and the export of moisture into the mid-troposphere through convective adjustment.

The moisture, which is exported from the planetary boundary layer by the meridional circulation, large-scale eddies and convective adjustment, condenses in the mid-troposphere of the model tropics, releasing its heat of condensation. Fig. 8.4a illustrates the vertical distributions of the rates of the upward transport of moisture by the meridional circulation and by large-scale eddies separately. This figure shows that the upward transport by large-scale eddies is significantly larger than that by the meridional circulation. In other words, the hydrologic processes in the rainbelt of the model tropics are enhanced markedly by the existence of large-scale eddies.

Nitta (1970) and Yanai *et al.* (1973) estimated how convection and condensation affect the water vapor content in the actual atmosphere. Their estimates are based upon the budget of water vapor in the polygons which connect the observational network in the neighborhood of the Marshall Islands. These estimates may be compared[8] with the contribution of convection and condensation shown in Fig. 8.3a. According to this comparison, their values are generally larger than the model values. This is reasonable because model values represent the zonal mean over the entire longitudinal span of the equator, whereas their values represent a local area in the western Pacific where moist convection is particularly intense. Although the general features of the vertical distributions in the model tropics agree reasonably well with those of the actual atmosphere, as estimated by Yanai *et al.*, there is one very significant difference. The distribution obtained by Yanai *et al.* shows no source of moisture near the earth's surface. On the other hand, a very intense net moisture source does exist in the planetary boundary layer of the model tropics. One of the reasons for this difference may be due to the difference in the scale of the small-scale eddies considered. Since the size of the polygons adopted in the studies of Nitta and Yanai *et al.* are much larger than the grid size used for this study, it is probable that their estimate of vertical convective transport includes the contribution of synoptic-scale eddies which are explicitly treated by the model. In fact, Murakami (1972) showed that the frequency spectra of vertical velocity depends upon the size of polygons chosen for analysis. Further studies are required to identify the cause of this discrepancy.

One can also examine the water balance in the model subtropics by use of Figs. 8.3b and 8.4b which show the budgets and the vertical fluxes of water vapor at 29N. According to these figures, the upward flux of water vapor by large-scale eddies in the model subtropics is much less than that in the model tropics. Furthermore, the meridional circulation transports moisture downward. Therefore, the supply of moisture from the planetary boundary layer into the mid-troposphere is relatively small and the moist convec-

[8] Divide the Q_2 value in Nitta's paper by the latent heat of evaporation and reverse the sign in order to compare his results with our distribution.

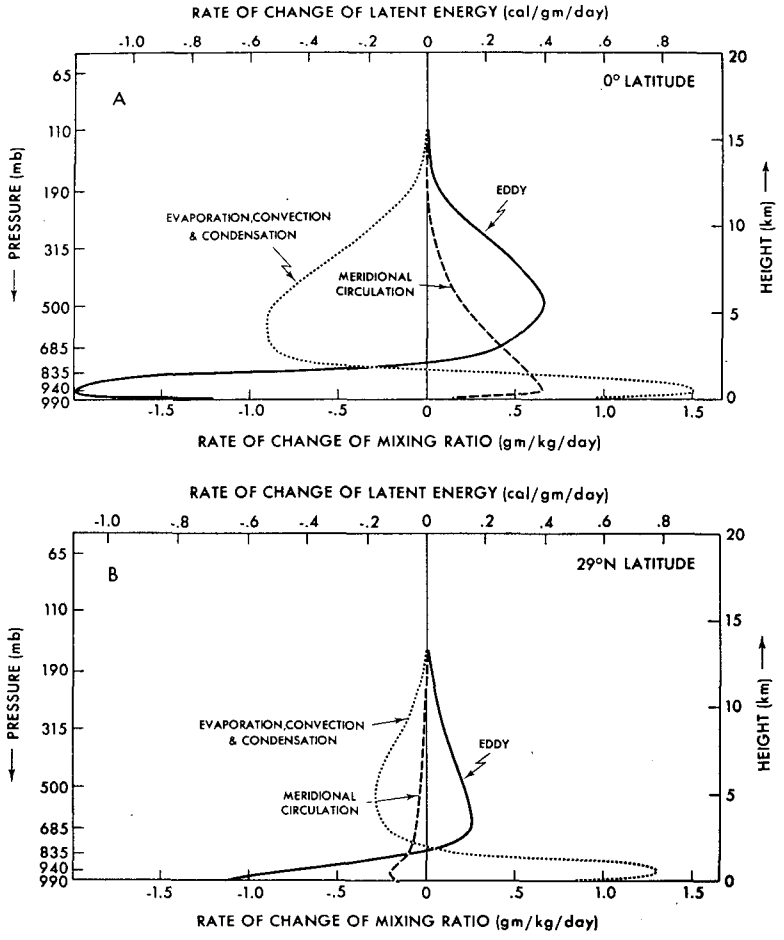

FIG. 8.3. Vertical distributions of the annual mean rate of moisture change due to various components of the water budget: top (A), zonal means at the equator; bottom (B), zonal means at 29N. Solid lines, the effect of large-scale eddies; dashed lines, the effect of meridional circulations; dotted lines; net contribution of condensation, dry and moist convection, and evaporation from the earth's surface.

tive activities are weak in the model subtropics. In short, very dry descending air seems to suppress the large-scale eddy activity as well as the hydrologic processes in the model subtropics.

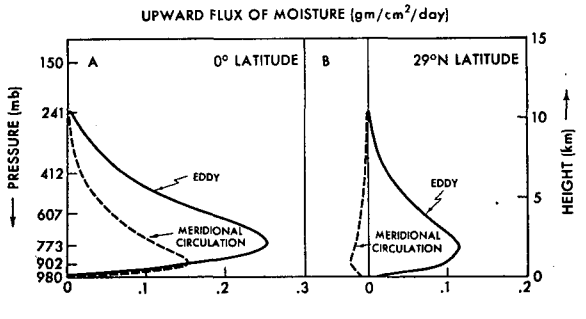

FIG. 8.4. Vertical distributions of the annual mean upward flux of moisture due to the meridional circulation (solid lines) and large-scale eddies (dashed lines) at the equator (A) and at 29N (B).

c. *Angular momentum balance*

It has been pointed out by Tucker (1965), Kidson *et al.* (1969) and others that large-scale eddies in the upper troposphere transport angular momentum across the equator from the winter to the summer hemisphere. This feature is successfully reproduced by Manabe *et al.* (1970) and Kasahara and Washington (1971) in the time integrations of their global models of the atmosphere. Similar features are evident in Fig. 8.5, which shows the distributions of the transport of angular momentum by stationary and transient components of large-scale eddies in the model atmosphere. In this figure

$$\text{Stationary transport} = 2\pi a \cos\theta \times \int_0^{p^*} (\bar{v}^{\lambda}_{t} - \bar{v}^{\lambda}_{t})(\bar{\mathfrak{R}}^{t} - \bar{\mathfrak{R}}^{t})\, dp, \quad (8.1)$$

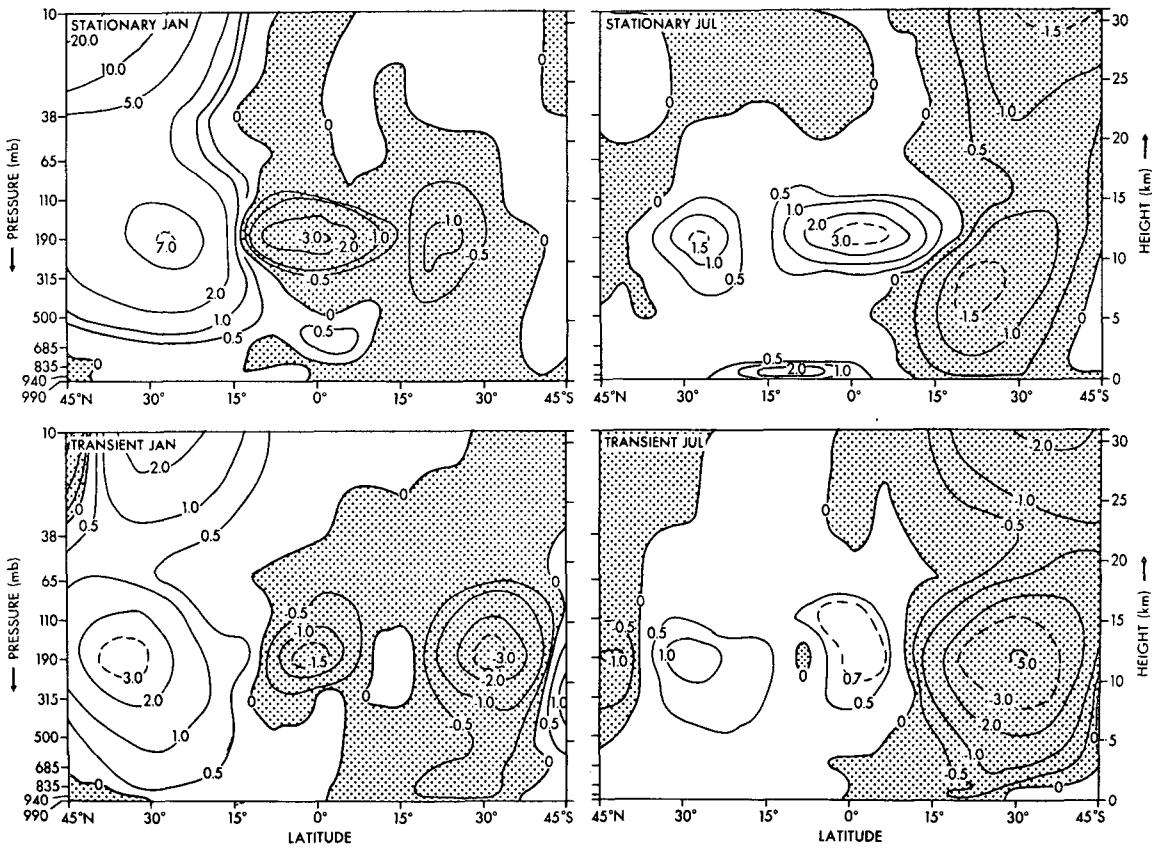

FIG. 8.5. Latitude-height distributions of the monthly mean northward transport of absolute angular momentum by eddies (10^{28} gm cm^2 mb^{-1} sec^{-1} day^{-1}): top, stationary components; bottom, transient components. Left, January; right, July. Negative areas are shaded.

$$\text{Transient transport} = 2\pi a \cos\theta \times \int_0^{p*} [(v-\overline{v}^{\lambda}) - (\overline{v}^{t} - \overline{v}^{\lambda,t})][(\mathfrak{R}-\overline{\mathfrak{R}}^{\lambda}) - (\overline{\mathfrak{R}}^{t} - \overline{\mathfrak{R}}^{\lambda,t})]dp, \tag{8.2}$$

where $\mathfrak{R}$ is absolute angular momentum defined by

$$\mathfrak{R} = a\cos\theta(u + a\Omega\cos\theta)$$

and Ω is the angular velocity of the earth. This figure indicates that the cross-equatorial transport of angular momentum is accomplished by both stationary and transient eddies. It is greatest in the upper troposphere where the kinetic energy of tropical disturbances is at a maximum. As shown in Section 5b, the quasi-stationary, cross-equatorial flow in the upper troposphere of the model tropics is most intense in January and July when the intense Hadley cell straddles the equator. In January, the S-shaped, cross-equatorial southerly wind predominates over Africa, the western Pacific and South America, and is responsible for the southward transport of angular momentum due to stationary eddies. In July, an intense northeasterly occupies most of Eastern Hemisphere and accounts for the large northward transport of angular momentum which is evident in Fig. 8.5. As pointed out by Dickinson (1971), large-scale asymmetries in the release of latent heat exist in the tropics, and these produce cross-equatorial flow and are responsible for the eddy flux of angular momentum across the equator. In Section 5b, it is shown that the asymmetric distribution of latent heat release generates an asymmetric pair of anticyclones around which the cross-equatorial flow meanders with the result that angular momentum is transported from one hemisphere to the other.

As Fig. 8.5 indicates, the transient eddies also transport angular momentum across the equator in the model atmosphere. Recently, Hayashi (1973) carried out a detailed analysis of the structure of the transient disturbances in the tropics of this model. According to his analysis, large-scale equatorial Rossby waves with a period of 10–20 days predominate in the upper troposphere of the model tropics. In July, the waves tilt from northeast to southwest and transport angular momentum from the Southern Hemisphere to the Northern Hemisphere. In short, his results indicate that Rossby waves are partly responsible for the cross-

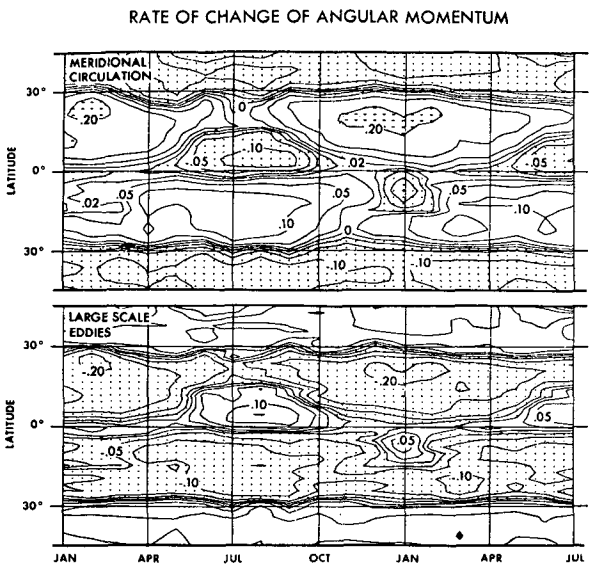

FIG. 8.6. Latitude-time distributions at the 190-mb level of the flux convergence of absolute angular momentum (10^{12} gm mb^{-1} sec^{-1} day^{-1}) due to the meridional circulation (top) and large-scale eddies (bottom).

equatorial transport of absolute angular momentum by transient eddies mentioned above.

The budget of angular momentum in the upper troposphere of the model tropics is essentially maintained by the balance between the effect of the meridional circulation and the effect of momentum transport by large-scale eddies. The contribution of subgrid-scale eddies is negligible as compared with these two effects. Fig. 8.6 shows the latitude-time distributions of the rates of change of angular momentum due to the advection of absolute angular momentum by meridional circulation and due to the momentum transport by large-scale eddies at the 190-mb level. It demonstrates how well the effect of the meridional circulation is compensated by that of large-scale eddies. The seasonal variation of the relative angular momentum of the zonal wind results from the small difference between these two effects.

The budget of angular momentum in the lower troposphere is somewhat different from that in the upper troposphere described above. The results of the present analysis indicate that the budget is dominated by the counteracting effects of the Coriolis force acting upon the meridional flow and the Reynolds stress in the planetary boundary layer. The seasonal variation of the zonal wind in the lower troposphere (Fig. 3.2) is in phase with that of the meridional circulation and is out of phase with the effect of the frictional stress.

9. Summary and conclusions

The global model of the atmosphere discussed here is capable of simulating major features of the seasonal variation of the tropical rainbelt. Over continental regions of the model, the rate of annual mean rainfall tends to be greatest over the equator. This is not the case over the eastern Pacific and the Atlantic Oceans. According to the comparison between the distribution of the rate of precipitation and that of sea surface temperature in the model tropics, the tropical rainbelts over the oceans tend to form in the areas of relatively warm sea surface temperatures. Based upon results from earlier numerical experiments as well as those of the present experiment, we speculate that the tendency for the tropical rainbelt to form away from the equator in certain oceanic regions of the model has not resulted from inherent characteristics of the model atmosphere, but is mainly caused by the belts of cold sea surface temperatures located at the equator in the model. In view of the very strong influence of sea surface temperature upon the distribution of rainfall in the model tropics, it would be very desirable to perform a series of numerical experiments designed to determine the relationship between the anomaly of sea surface temperature and the distribution of precipitation rate in the tropics.

The long belt of heavy precipitation, which is considered to be one of the characteristic features of the tropical rainbelt, emerges only when the rate of precipitation is averaged over sufficiently long periods of time. The distribution of 6-hr rainfall in the model tropics reveals a cellular rather than a zonal structure. In other words, the tropical rainbelt of the model consists of a chain of cells of heavy precipitation accompanying synoptic-scale disturbances. The characteristic horizontal dimensions of these cells vary, but they average about 1000 km in diameter. Some of these cells may be identified with cloud clusters as detected in satellite pictures.

In the lower troposphere of the model, the seasonal variation of the location of the ITCZ and of the flow field around it is highly realistic. For example, the complete reversal of the direction of surface flow over the northern Indian Ocean from January to July is successfully reproduced by the model.

The model also simulates some of the observed features of the flow field in the upper troposphere such as:

1) The mid-oceanic troughs which intensify in summer.
2) The easterly jet prevailing during the period of the summer Indian Monsoon.
3) The anticyclonic pairs which straddle the equator in the western Pacific and other regions.
4) The equatorial westerlies over the eastern Pacific and the Atlantic (manifestations of the Walker circulation in the Pacific and a similar circulation in the South America-Atlantic region).

The eddy kinetic energy in the model tropics is at a maximum around the 200-mb level in agreement with features of the actual tropics. The analysis of the

seasonal variation of eddy kinetic energy in the model tropics indicates significant differences between the upper and lower troposphere. In the upper troposphere of the model, the eddy kinetic energy at the equator is greatest around January and July. In the lower troposphere, the zonal belt of maximum eddy kinetic energy moves from one hemisphere to the other with respect to season in approximately the same way as the movement of the tropical rainbelt. The magnitude of the eddy kinetic energy, however, does not necessarily vary in proportion to the rate of rainfall. It is particularly large at about 10N in July. Further study is required to determine whether the development of the tropical disturbances has latitudinal preference or not.

In the lower troposphere of the model tropics, the kinetic energy of the transient eddies is large over certain oceanic regions where sea surface temperatures are relatively high, particularly over the western Pacific in the summer hemisphere. (In the upper troposphere, the correspondence between the two quantities is less obvious but is discernible.) This result suggests that the relatively warm sea surface temperatures tend to encourage the development of tropical disturbances in the model tropics. The areas of large kinetic energy of transient eddies mentioned above coincide very well with the areas of frequent formation of tropical cyclones in the actual tropics.

The analysis of energetics of the disturbances in the model tropics indicates that the primary source of eddy kinetic energy is the conversion of eddy available potential energy and the secondary source is the energy supplied from middle latitudes through pressure interaction. The contribution of pressure interaction is largest in the subtropics and affects significantly the budget of eddy kinetic energy there.

The belt of large eddy conversion in the model tropics moves between the two hemispheres with respect to season in a manner similar to the tropical rainbelt. It is located in the tropics of the summer hemisphere. On the other hand, the contribution of pressure interaction is largest in the subtropics of the winter hemisphere and there it supplements the contribution of eddy conversion which is relatively small in that season.

The rate of eddy conversion in the model tropics is particularly large in certain oceanic regions where sea surface temperatures are relatively high, particularly in the summer-hemispheric part of the western Pacific. The warm sea surface temperatures increase the supply of moisture in the lower troposphere, raise the temperature of the warm anomaly in the upper troposphere through the mechanism of the convective adjustment, and thus encourage the release of available potential energy.

The analysis of the budget of angular momentum in the model tropics reveals that large-scale disturbances transport angular momentum across the equator from the winter to the summer hemisphere. The change of angular momentum due to this effect is compensated by the change due to the advection of absolute angular momentum by the meridional circulation. The small difference between these two opposing contributions accounts for the change of zonal wind in the upper troposphere of the model tropics.

In the lower troposphere of the model tropics, the effect of large-scale eddies on the budget of angular momentum is relatively small. The contribution of meridional circulation is almost compensated by the exchange of angular momentum between the earth's surface and the atmosphere.

According to the analysis of heat budget, the heating due to moist and dry convection is counter-balanced by the cooling due to meridional circulation and radiative transfer in the model tropics. It is shown that both large-scale eddies and meridional circulation transport latent heat upward and maintain moist convection in the model tropics. Particularly, the former is found to be very effective in transporting moisture from the planetary boundary layer into the middle and upper troposphere.

The heat balance in the model subtropics is maintained quite differently from the tropical budget described above. In the subtropics, meridional circulation has a warming effect because of the adiabatic heating of descending air. Furthermore, moist convection penetrates much less in the subtropics than in the tropics. The overall balance is maintained between the cooling due to radiation and the heating due to meridional circulation and dry and moist convection.

In general, the basic features of the general circulation in the model tropics are very realistic despite the extreme idealizations adopted in the formulation of the parameterization of moist convection. There are, however, various systematic differences between the structure of the model atmosphere and that of the actual atmosphere. For example, the intensity of the easterlies in the stratosphere of the model tropics tends to be too strong. The vertical distribution of static stability in the troposphere of the model tropics is significantly different from the observed distribution as described in Section 3. The relative humidity in the lower troposphere of the model is systematically higher than the observed humidity. Since the moist convective adjustment strongly influences the distribution of static stability and relative humidity, it is possible that improvement of the parameterization of moist convection could rectify the last two of the difficulties mentioned above.

Recently, Miyakoda *et al.* (1973) attempted a numerical prediction of the tropical circulation by use of a model which is very similar to the one used for this study. They observed a rapid deviation of the state of the model atmosphere from the observed state during the first day of the time integration. In other words, the model atmosphere underwent a process of rapid adjust-

ment from a realistic state to a state consistent with the systematic bias of the model. Their experience indicates that there is a significant difference between the behavior of the model and the actual atmosphere.

In the course of this study, we have noted other shortcomings of the model. For example, the horizontal distribution of vertical velocity reveals an irregular, grid-scale pattern which is not sufficiently resolved by the finite-difference representation of the model. Furthermore, it was necessary to suppress the excessive growth of inertial gravity waves by the periodic application of the so-called "Euler backward scheme" proposed by Matsuno (1966a) during the course of the numerical time integration of the model (Holloway and Manabe, 1971). These difficulties partly stem from the abrupt execution of the convective adjustment in response to the fulfillment of the conditions for moist convection. The various difficulties described above underscore the necessity for further improvement in the parameterization of moist convection, as well as in other components of the model, for the better simulation of the tropical circulation.

Acknowledgments. The authors are very much indebted to Dr. J. Smagorinsky who has given them many valuable suggestions and wholehearted support throughout the course of this study. We acknowledge Dr. Y. Hayashi who has given us many valuable interpretations of the results obtained from the numerical experiments. The authors wish to thank D. Daniel for his effective day-by-day management of the model's integration. We are grateful to Drs. Y. Kurihara and T. Gordon and Prof. J. C. Sadler who gave many useful comments on the results of this study. It is a pleasure to acknowledge Messrs. L. Dimmick, P. Tunison and Mrs. E. D'Amico whose assistance was indispensable in the preparation of the figures and the manuscript.

REFERENCES

Bates, J. R., 1970: Dynamics of disturbances on the intertropical convergence zone. *Quart. J. Roy. Meteor. Soc.*, **96**, 677–701.

——, 1971: Reply (to comments by Pike). *Quart. J. Roy. Meteor. Soc.*, **97**, p. 351.

Bjerknes, J., 1969: Atmospheric teleconnections from the equatorial Pacific. *Mon. Wea. Rev.*, **97**, 163–172.

——, L. J. Allison, E. R. Kreins, F. A. Godshall and G. Warnecke, 1969: Satellite mapping of the Pacific tropical cloudiness. *Bull. Amer. Meteor. Soc.*, **50**, 313–322.

Bryan, K., 1969: Climate and ocean circulation, Part 3, The ocean model. *Mon. Wea. Rev.*, **97**, 806–827.

Budyko, M. I., 1956. *Teplovoi Balans Zemnoi Poverkhnosti.* (English transl.: Stepanova, N. A., 1958: *The Heat Balance of the Earth's Surface.* Office of Technical Services, U. S. Dept. of Commerce, Washington, 69 pp.). Leningrad, Gidrometeoizdat.

——, 1964: Atlas teplovogo balansa zemnogo shara, mezhuduvedomstvennyi geofizicheskii komo tet pri prizidum. *Akad. Nauk SSSR Gl. Geofiz. Observ.*

Charney, J. G., 1966: Some remaining problems in numerical weather prediction. *Proceedings of Conference,* Traveler's Research Center, Hartford, Conn., 1–10.

Dickinson, R. E., 1971: Cross equatorial eddy momentum fluxes as evidence of tropical planetary wave sources. *Quart. J. Roy. Meteor. Soc.*, **97**, 554–558.

Gray, W. M., 1968: Global view of the origin of tropical disturbances and storms. *Mon. Wea. Rev.*, **96**, 669–700.

Hayashi, Y., 1970: A theory of large-scale equatorial waves generated by condensation heat and accelerating the zonal wind. *J. Meteor. Soc. Japan*, **48**, 140–160.

——, 1973: Spectral analysis of tropical disturbances appearing in a GFDL general circulation model. To be submitted to *J. Atmos. Sci.*

Holloway, J. L., Jr., and S. Manabe, 1971: Simulation of climatology by a global general circulation model. *Mon. Wea. Rev.*, **99**, 335–370.

Hydrographic Office, U. S. Navy, 1944: *World Atlas of Sea Surface Temperature,* 2nd ed. H. O. Publ. No. 225.

——, 1964: *World Atlas of Sea Surface Temperature,* 2nd ed. H. O. Publ. No. 225, with supplements.

Johnson, D. H., 1969: The role of the tropics in the global circulation. *Proc. Joint Conf. Global Circulation of the Atmosphere,* London, Roy. Meteor. Soc.

Kasahara, A., and W. N. Washington, 1971: General circulation experiments with a six layer NCAR model, including orography, cloudiness and surface temperature calculation. *J. Atmos. Sci.*, **28**, 657–701.

Kidson J. W., D. G. Vincent and R. E. Newell, 1969: Observational studies of the general circulation of the tropics. *Quart. J. Roy. Meteor. Soc.*, **95**, 258–287.

Krishnamurti, T. N., 1969: An experiment in numerical prediction in equatorial latitudes. *Quart. J. Roy. Meteor. Soc.*, **95**, 594–620.

Kurihara, Y., and J. L. Holloway, Jr., 1967: Numerical integration of a nine-level global primitive equations model formulated by the box method. *Mon. Wea. Rev.*, **95**, 509–530.

Mak, M. K., 1969: Laterally driven stochastic motions in the tropics. *J. Atmos. Sci.*, **26**, 41–64.

Malkus, J. S., 1962: Large scale interactions. *The Sea,* Vol. 1, *Physical Oceanography,* M. N. Hill, Ed., New York, Interscience, 88–294.

Manabe, S., 1969a: Climate and the ocean circulation, Part 2, The atmospheric circulation and the effects of heat transfer by ocean currents. *Mon. Wea. Rev.*, **97**, 775–805.

——, 1969b: Climate and ocean circulation, Part 1, The atmospheric circulation and hydrology of the earth's surface. *Mon. Wea. Rev.*, **97**, 739–774.

——, and R. T. Wetherald, 1967: Thermal equilibrium of the atmosphere with a given distribution of relative humidity. *J. Atmos. Sci.*, **24**, 241–259.

——, and J. Smagorinsky, 1967: Simulated climatology of a general circulation model with a hydrologic cycle, 2, Analysis of the tropical atmosphere. *Mon Wea. Rev.*, **95**, 155–165.

——, and R. F. Strickler, 1964: On the thermal equilibrium of the atmosphere with convective adjustments. *J. Atmos. Sci.*, **21**, 361–385.

——, and T. B. Terpstra, 1974: The effects of mountains on the general circulation of the atmosphere as identified by numerical experiments. *J. Atmos. Sci.*, **31**, 3–42.

——, and J. L. Holloway, Jr., 1970: Climate modification and a mathematical model of atmospheric circulation. *A Century of Weather Progress,* Boston, Amer. Meteor. Soc., 157–164.

——, —— and H. M. Stone, 1970: Tropical circulation in a time-integration of a global model of the atmosphere. *J. Atmos. Sci.*, **27**, 580–613.

——, J. Smagorinsky and R. F. Strickler, 1965: Simulated climatology of a general circulation model with a hydrologic cycle. *Mon. Wea. Rev.*, **93**, 769–798.

——, D. G. Hahn and J. L. Holloway, Jr., 1974: The seasonal variation of stratospheric circulation as simulated by a global model of the atmosphere (in preparation).

Matsuno, T., 1966a: Numerical integration of primitive equations by use of a simulated backward difference method. *J. Meteor. Soc. Japan*, **44**, 76–84.

——, 1966b: Quasi-geostrophic motions in the equatorial area. *J. Meteor. Soc. Japan*, **44**, 25–43.

Mintz, Y., 1965: Very long term global integration of the primitive equation of atmospheric motion. WMO Tech. Note 66, *Proc. WMO-IUGG Symp. Research and Development Aspects of Long Range Forecasting*, 141–161.

——, 1968: Very long-term global integration of the primitive equations of atmospheric motion: An experiment in climate simulation. *Meteor. Monog.*, **8**, No. 30, 20–36.

——, and G. Dean, 1952: The observed mean field of motion of the atmosphere. *Geophys. Res. Papers*, No. 17, 65 pp.

Miyakoda, K., J. C. Sadler and G. D. Hembree, 1973: An experimental prediction of the tropical atmosphere for the case of March 1965 (manuscript in preparation).

Möller, F., 1951: Viertel Jahrs Karten des Niederschlags für die Ganze Erde. *Petermanns Geograph. Mitt.*, **95**, 1–7.

Murakami, M., 1972: Intermediate-scale disturbances appearing in the ITCZ zone in the tropical western Pacific. *J. Meteor. Soc. Japan*, **50**, 454–464.

Newell, R. E., J. W. Kidson, D. G. Vincent and G. J. Boer, 1972: *The General Circulation of the Tropical Atmosphere and Interactions with Extratropical Latitudes*. The MIT Press, 258 pp.

Nitta, T., 1970: A study of generation and conversion of eddy available potential energy in the tropics. *J. Meteor. Soc. Japan*, **48**, 524–528.

——, 1972: Energy budget of wave disturbances over the Marshall Islands during the year of 1956 and 1958. *J. Meteor. Soc. Japan*, **50**, 71–84.

Oort, A. H., and E. Rasmusson, 1971: Atmospheric circulation statistics. NOAA Prof. Paper No. 5, 323 pp.

Phillips, N. A., 1956: The general circulation of the atmosphere: A numerical experiment. *Quart. J. Roy. Meteor. Soc.*, **82**, 123–164.

——, 1957: A co-ordinate system having some special advantage for numerical forecasting. *J. Meteor.*, **14**, 184–185.

Pike, A. C., 1970: A numerical study of tropical circulations. Sci. Rept. AFCRL-68-0593, 129 pp.

——, 1971: Comments (on a paper by Bates). *Quart. J. Roy. Meteor. Soc.*, **97**, p. 350.

Reed, R. J., and C. L. Vleck, 1969: The annual temperature variation in the lower tropical stratosphere. *J. Atmos. Sci.*, **26**, 163–167.

Richards, M. E., 1967: The energy budget of the stratosphere during 1965. Rept. No. 21, Planetary Circulation Project, Dept. of Meteorology, MIT.

Sadler, J. C., 1972: Mean upper tropospheric circulation of the tropics. Preliminary pre-publication, Dept. of Meteorology, University of Hawaii, NSF Grant GA36301.

Smagorinsky, J., 1963: General circulation experiments with primitive equations, 1. The basic experiment. *Mon. Wea. Rev.*, **93**, 99–164.

Taylor, V. R., and J. S. Winston, 1968: Monthly and seasonal mean global charts of brightness from ESSA 3 and ESSA 5 digitized pictures, February 1967–February 1968. ESSA Tech. Rept. NESC46, National Environmental Satellite Center, Washington, D.C.

Tucker, G. B., 1965: The general tropospheric wind regime. *Quart. J. Roy. Meteor. Soc.*, **91**, 140–150.

USSR Academy of Sciences, Dept. of Geophysics and Cartography, 1964: *Physical Geographical Atlas of the World.*

Webster, P. J., 1972: Response of tropical atmosphere to local, steady forcing. *Mon. Wea. Rev.*, **100**, 518–541.

Yamasaki, M., 1969: Large-scale disturbances in a conditionally unstable atmosphere in low latitudes. *Papers Meteor. Geophys.*, **20**, 289–336.

Yanai, M., S. Esbensen and J.-H., Chu, 1973: Determination of bulk properties of tropical cloud clusters from large-scale heat and moisture budgets. *J. Atmos. Sci.*, **30**, 611–627.